MODELING SURGICAL INTERVENTIONS IN THE MITRAL VALVE WITH THE FINITE ELEMENT METHOD

by

Sandeep Abhay Urankar

B.Tech., Indian Institute of Technology Kanpur, 2004

M.S., University of Pittsburgh, 2006

Submitted to the Graduate Faculty of

Swanson School of Engineering in partial fulfillment

of the requirements for the degree of

Master of Science in Bioengineering

University of Pittsburgh

2008

UNIVERSITY OF PITTSBURGH

SWANSON SCHOOL OF ENGINEERING

This thesis was presented

by

Sandeep Abhay Urankar

It was defended on

September 24th, 2008

and approved by

Tin-Kan Hung, Professor, Bioengineering Department

Michael Lovell, Professor, Industrial Engineering Department

Thesis Adviser: Jeen-Shang Lin, Associate Professor, Civil and Environmental Engineering Department

MODELING SURGICAL INTERVENTIONS IN THE MITRAL VALVE WITH THE FINITE ELEMENT METHOD

Sandeep Abhay Urankar, M.S.

University of Pittsburgh, 2008

The behavior of mitral valve tissue is very complex because of its material composition, geometric layout and loading environment. Due to recent advances in the constitutive modeling of mitral valve material, particularly in the area of incorporating the collagen fibers with the continuum tissue matrix, we are able to now simulate the behavior of the mitral valve under various loading and surgical conditions. Further, advance in FEM computational formulation also enables us to accurately simulate the nature of the incompressible material as representative of the mitral valve tissue which was a difficult proposition only a few years ago.

In this thesis, we first implemented a constitutive relation specifically developed for mitral valve tissue into a commercial finite element software – LSDYNA. The geometry of the mitral valve and it's chordae were modeled via previously published anatomical measurements and our observations during animal experiments. We first simulated the motion of a porcine mitral valve under normal conditions that enabled us to make inferences about the state of stress of the mitral valve, i.e. we indentified sites of high stress and consequently locations of high failure possibility. Having modeled a healthy mitral valve we then modeled a prolapsed leaflet by removing chordae attached to the anterior leaflet of the valve. Further we proceeded to

simulate a novel surgical procedure used to repair prolapse. The effects of surgical repair in term of the stresses the valve were quantified in comparison to its natural state.

In our constitutive equations we included the material fiber direction, i.e. the direction of the collagen fibers in the mitral valve tissue. In accordance with stress modulated growth laws, we assumed that the fiber direction will tend to align with the maximum principal direction of stress as the tissue remodels under the influence of new external forces after surgical alteration. This study shows the change in principal stress directions due to surgical alteration, and therefore is an indicator of remodeling to follow. Thus, the ability, as demonstrated by this study, to predict these alteration may be one way to devise a strategy for minimizing fiber reorientation and thereby prolong the effects of surgical intervention or even avoid future re-intervention.

TABLE OF CONTENTS

LIST OF TABLES

LIST OF FIGURES

PREFACE

I would like to acknowledge Dr. Giovanni Speziali for introducing me to his project in surgery, that of repair of mitral valves using his novel techniques. It is my sincere hope that mathematical techniques such as the ones I used will serve a bigger role in the planning and evaluation of surgery in the future.

I appreciate my mentor and advisor, Professor Michael Lovell, over the last four years, for his continuing funding, support, friendship and advice. Without his constant encouragement and guidance, this work would not have been possible. After he left two months ago to become the Dean of School of Engineering at University of Wisconsin, Milwaukee, I have enjoyed and appreciated the assistance and guidance of Professor Jeen-Shang Lin. Professor Tin-Kan Hung's comments and suggestions are also deeply appreciated.

I would like to thank my parents for their constant support throughout my education. For their understanding when I made choices that they didn't quite understand and most of all for encouraging me to think, and think independently from a very early age. My sister for challenging me always to do my best, even though she didn't know it.

Last but not the least I would like to thank Kristy for tolerating me through this long arduous process. For her help with everything, from biscotti for the defense to formatting of the thesis. Thanks.

1.0 INTRODUCTION

1.1 THE MITRAL VALVE: FUNCTION, ANATOMY AND COMPOSITION

The mitral valve regulates blood flow between the left ventricle and the left atrium. It consists of two leaflets, anterior and posterior, attached to the papillary muscles in the left ventricle via tendons known as chordae tendinae or simply chordae. (see Figure 1)

The tendons serve to hold the valve in place as the left ventricle develops pressure during systole. If the chordae rupture, the valve leaflets prolapse (Hayek E. 2005) into the left atrium causing the blood to flow into the atrium in systole which is undesirable. The papillary muscles are believed to contract so as to assist the opening of the valve in early diastole, and in systole to increase tension in the chordae so that they don't prolapse into the atrium and It has long been assumed that the tips of the papillary muscle move toward the apex of the heart during contraction, but recent fluoroscopic data suggests that there is little vertical excursion while their lateral motion of follows the gross motion of the ventricle. (Dagum 2000) implying very little contribution to the coaption process.

The closure remains mostly a passive process driven by the pressure difference in the blood and to an extent by the forces generated by the flow (for e.g. the vortex formation behind the mitral leaflets in diastole are thought to aid in the opening of the valve)

The chordae can be divided into three main categories: marginal, basal and strut chords. Marginal chords originate from the papillary muscles and attach to the free edge of the zone of opposition. They are more or less uniformly distributed along the free edge making proper

coaption possible. The basal attachments generally occur between the ventricular rough end of the posterior leaflet and the ventricle wall. Basal chords tend to have a thick belly of their own. On the anterior leaflet, there are typically two or three prominent thick chords which attach the ventricular rough end to the papillary muscles. These chords are thought to carry a lot more tension than the marginal chords which are thinner, highly branched and stiffer.

The circumference of the mitral valve attachment to the heart is referred to as the annulus. The annulus is a collective reference to a host of different material, for example the basal attachment of the posterior leaflet is mostly what is referred to as annulus material but the anterior leaflet's basal attachment is quite different, it is continuous with the septum and the wall of the ascending aorta (which it is adjacent to). Near the zone where the two leaflets attach to one another, the anterior annulus is known as the trigone.

The anterior leaflet is the taller leaflet and sits adjacent to the aorta, however it's annular length is much smaller. In a way, it tucks under the posterior leaflet during closure pushing the posterior leaflet towards the outside of the valve (K. Kunzelman 1994). It is attached to the annulus almost in a straight line, and therefore is hinged more freely.

The posterior leaflet is longer at the annulus and significantly arched, but shorter in height. The free edge of this leaflet is bunched into several folds along the line of opposition (see Figure 2).

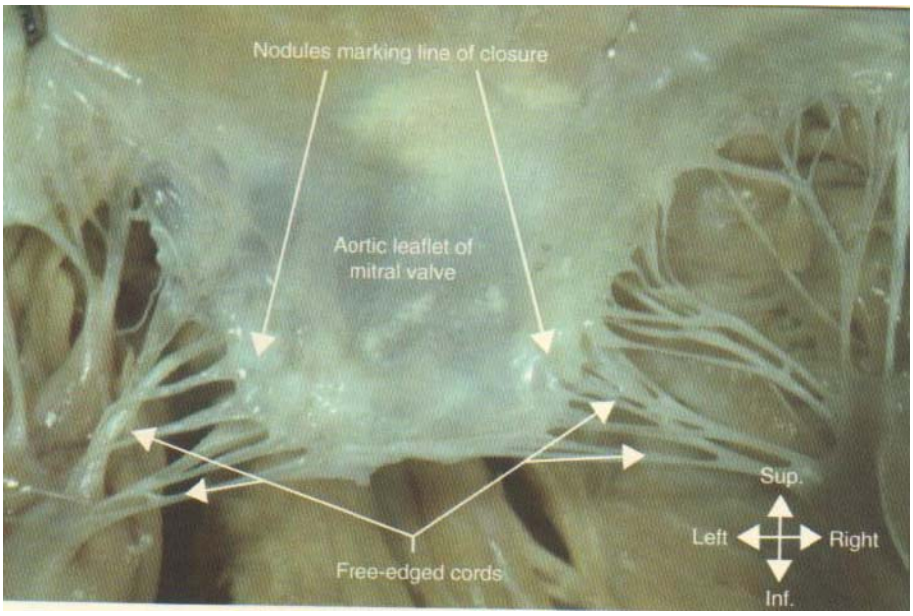

Figure 1: Uniform marginal chordate, reproduced from: (Wilcox 2005)

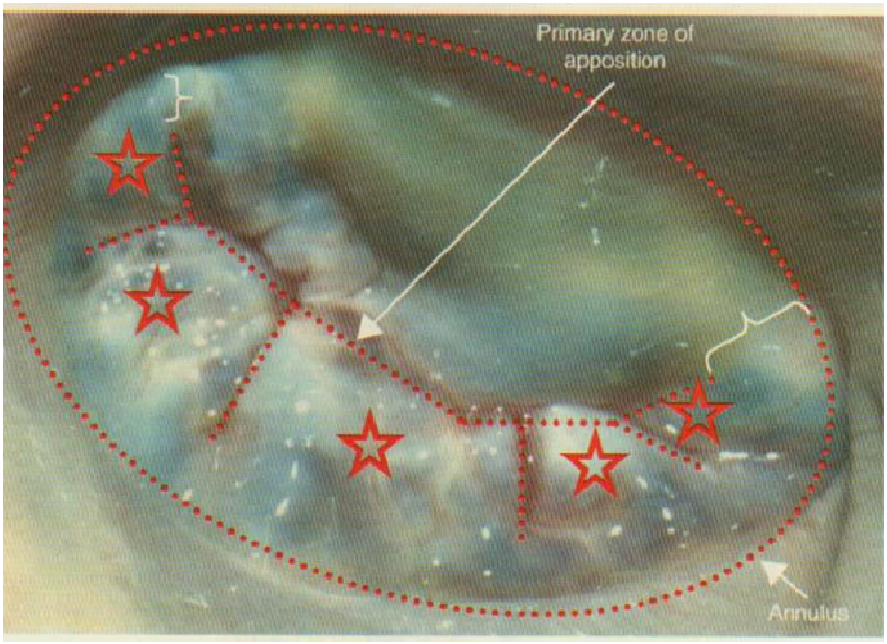

Figure 2: Folds at the free edge, reproduced from: (Wilcox 2005)

The mitral valve leaflets can be thought of as composed of three layers of membranes:

1. Spongiosa
2. Fibrosa
3. Ventricularis and atrialis

The spongiosa is a layer that consists of proteoglycans, elastin and connective tissue cells. It contains relatively much lesser collagen fibers as compared to the other two layers. The fibrosa (named due to its fibrous nature) consists primarily of collagen fibers and forms the core of the valve responsible for bearing load. The ventricularis and the atrialis wrap the spongiosa and the fibrosa in a thin layer of elastin fibers. As the name suggests the ventricularis is the elastin layer on the ventricular side and the atrialis is the elastin layer of the atrial side. The ventricularis has a higher collagen content and is more likely to thicken with age.

The annulus material is primarily composed of highly bundled collagen fibers coupled with elastin fibers. In the trigones the annulus material is reinforced by more fibers.

Since we are interested in the structural analysis of the mitral valve, we will assume the mitral valve material to be composed of oriented crimped collagen fibers, which take load in tension, immersed in a homogeneous matrix composed of every other constituent in the valves. It is possible to experimentally obtain the direction of these oriented fibers via SALS (Cochran 1991). Cochran et al. prepared a approximate map of the mean collagen fiber orientation In the valve, given in Figure 3

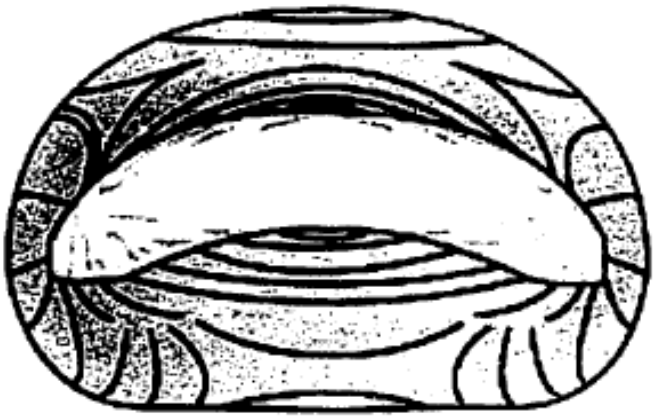

Figure 3: Approximation of mean collagen fiber orientation, source: (Cochran 1991)

1.2 DESCRIPTION OF SOFT TISSUE BEHAVIOR

The mechanics of soft tissue results from an integrated response of many components that compose the tissue (Fung 1993). Sometimes it is essential to calculate stress/strain at a component level, that is, to work at the cellular level. For example, when studying the flow of a single cell through a micro pipette. On the other hand, on many occasions, such as when trying to calculate stress distribution in an artery wall, (Taber 2004) it is sufficient to adopt a continuum mechanics approach. Such an approach is justified when the scale of the problem is much larger than the scale of the individual components that constitute the tissue.

In this thesis, we are interested primarily in the characterization of mitral valve tissue and the chordae tedinae in a continuum mechanics framework. But before we dwell into the specifics of mitral valve tissue, it would be instrumental to describe some general characteristics of soft tissue and appreciate the theoretical foundations for solving soft tissue mechanics problems.

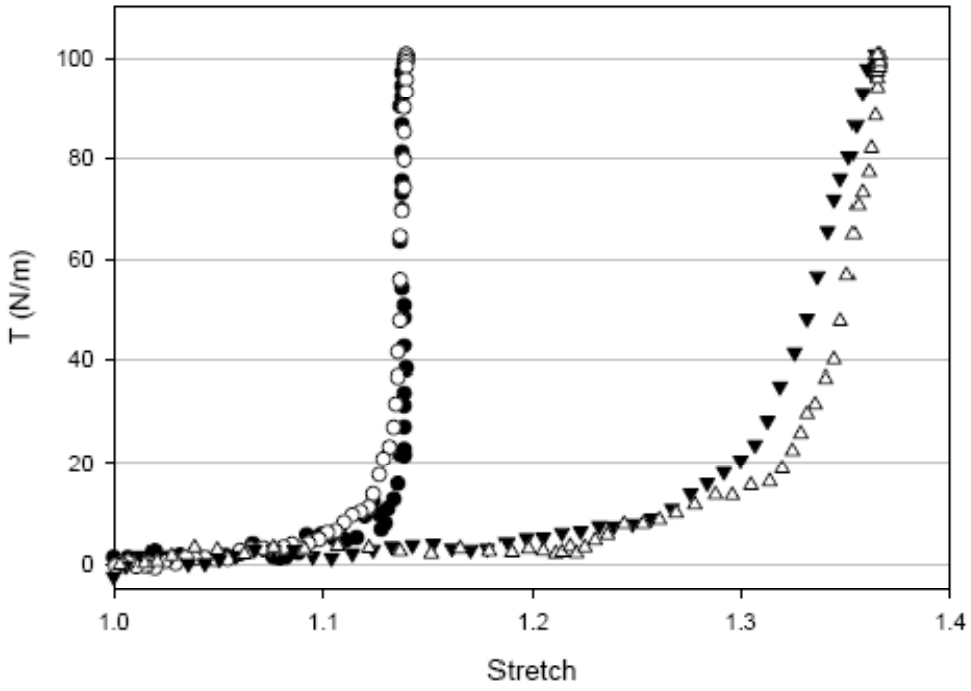

Figure 4: Hysteresis and Anisotropy. circles - in fiber direction, triangles - cross fiber direction

source: (Grashow 2002)

Figure 4 shows typical behavior of passive valve tissue in response to loading. The tissue sample excised from the belly of a mitral valve, is composed of oriented collagen fibers in a thin sheet of fibrous elastin. The stress-stretch response shows typical nonlinear behavior of soft tissue. At low stretch, the tissue is considerably less stiff but as the stretch increases more and more collagen fiber are recruited (initially crimped) to give a stiffer response. Also evident is the hysteresis and anisotropy of valve tissue. The response in the fiber direction is different from other directions. In summary, soft tissue is nonlinear, inelastic, and anisotropic and undergoes finite strain.

The theoretical framework for analysis of such a material was pioneered by great scientists such as Euler, Navier, Cauchy, Green etc. (Truesdell 1966).

Under the continuum assumption, it involves the simultaneous solution of five classes of relations:

1. Kinematics: displacements and quantities derived from it.
2. Forces: traction and stress
3. Balance relations: mass balance, momentum balance etc.
4. Constitutive relations: Material behavior
5. Boundary and initial conditions: necessary for solving differential equations

The theoretical framework was further developed by Truesdell(1965), Malvern(1969), Chadwick(1976), Spencer(1980) and Bowen(1989) into it's current form, referred to as continuum mechanics. This thesis uses all five of the above mentioned relations to describe the behavior of the mitral valve and it's chordae. Each relation, as it applies to our problem will be described in detail in the following sections.

1.2.1 Kinematics

Kinematics is a description of the position, displacement and strain of the material in question. Soft tissue undergoes large deformation, and therefore geometric nonlinearity has to be accounted for. Note that the nonlinearity discussed in Figure 4 is material nonlinearity and will be discussed in constitutive relationships. In particular, a constitutive relation capable of modeling the behavior of the mitral valve will be discussed and implemented.

For deformation to be measured, we need to refer to a reference configuration. This configuration need not be stress free. In fact, most unloaded soft tissue contain residual stress (see Figure 5)

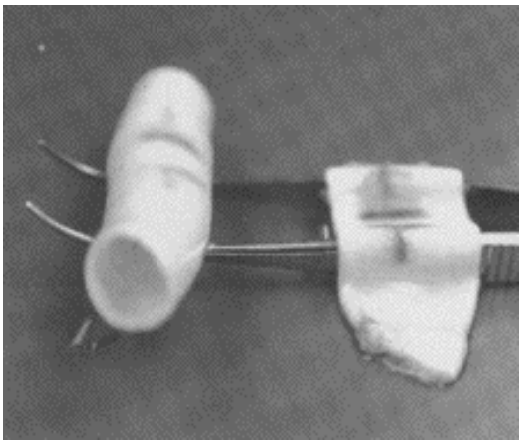

Figure 5: Pre-stressed and stress-free states of an artery, source: (Holzapfel 2000)

Despite the residual stress, the unloaded state is a good choice for a reference configuration. Referring to what is commonly referred to as the continuum "potato" (see Figure 6). Consider the deformation of a point P in the un-deformed body Ko(B) at time t=0 into the point P* in the deformed configuration Kt(B) at time t. The point P is located at the material coordinate X and P* is located at the spatial coordinate x. In general the coordinates systems have origins O and o respectively that may be in relative motion with respect to one another.

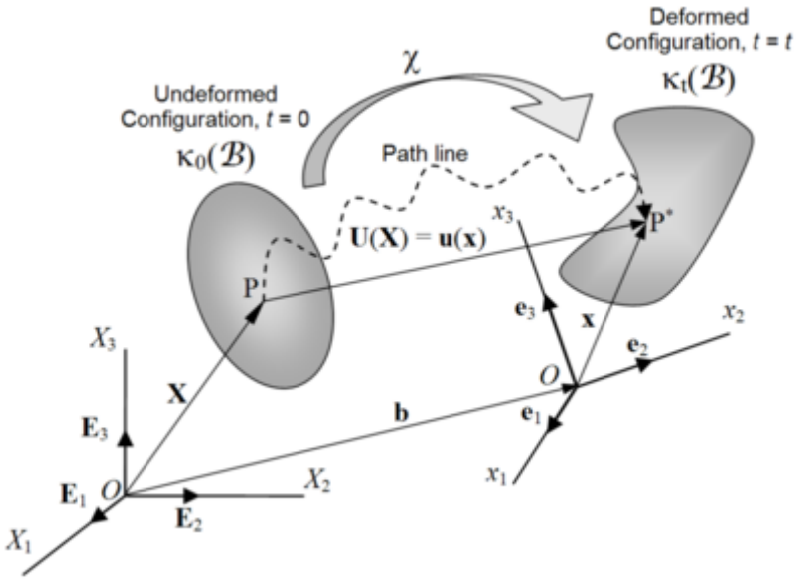

Figure 6: Un-deformed and deformed configurations

The coordinate transformation between the coordinate systems is given by:

$$dr = F.dR = dR.F^T$$

Where:

dr and dR are differential line elements in x and X respectively

$F = \frac{\delta xi}{\delta Xi}$ is the deformation gradient tensor.

The deformation gradient tensor F is decomposed into:

$C = F^T.F, B = F.F^T$,

Where:

C and B are the right and left Cauchy-Green deformation tensors.

The Lagrangian strain tensor **E** can be given by:

$$2E = C - I = F^T.F - I$$

The Eulerian strain tensor **e** can be given by:

$$2e = I - B^{-1} = I - F^{-T}.F^{-1}$$

The strains relate to the displacements via strain displacement relations:

$$E = \frac{1}{2}[\nabla u + (\nabla u)^T + (\nabla u).(\nabla u)^T]$$

$$e = \frac{1}{2}[\overline{\nabla} u + (\overline{\nabla} u)^T - (\overline{\nabla} u).(\overline{\nabla} u)^T]$$

Where:

$\nabla u = \frac{\delta u}{\delta R}$ and $\overline{\nabla} u = \frac{\delta u}{\delta r}$, u is the displacement vector

The strain displacement relationship shows that strain measures (which will be used in building our constitutive relations) can be obtained from displacement and the displacement

gradient. The relation also illustrates the geometric nonlinearity is rooted in the quadratic terms in the relation.

The lagrangian stretch ratio $\Omega(N)$for an element that occupies a specified direction N in the un-deformed body can be given by:

$$\Omega(N)^2 = \mathrm{N.C.N}$$

The lagrangian extension ratio (analogous to engineering strain) can be given by:

$$E^*(N) = \frac{ds - dS}{dS} = \Omega(N) - 1$$

Where: dS and ds are the lengths of differential line elements before and after deformation.

The Eulerian stretch ratio λ(n) for an element that occupies a specified direction n in the deformed body can be given by:

$$\lambda_{(n)}^{-2} = n.B^{-1}.n$$

The Eulerian extension ratio (analogous to true strain) can be given by:

$$e^*(n) = \frac{ds - dS}{ds} = 1 - \frac{1}{\lambda(n)}$$

The dilatation ratio (ratio of the deformed to the un-deformed volume) is defined as:

$$J = \frac{dv}{dV} = \det F$$

Soft tissue is usually assumed to be incompressible, therefore J =1. This is a constraint that needs to be enforced in the constitutive relations.

Some of the important quantities and relations in kinematics that will be used in this thesis were stated in this section. For derivations and alternative descriptions see (Fung 1993).

1.2.2 Forces, tractions and stress

Humphrey introduces stress as, “an intuitive concept whose precise definition is not necessarily straightforward”. For an in-depth discussion the reader is referred to (Fung 1993)

Stress is only a measure of force acting over an oriented area. It is in fact a two dimensional tensor (because of the presence of two orientations, that of area and force). Cauchy stress denoted by **t** is then a tensor that transforms the orientation **n** of an area element **da** in the deformed configuration into a traction vector $T^{(n)}$ such that:

$$T^{(n)} = n.t \quad T_j^{(n)} = n_i t_{ij}$$

Cauchy stress is a true stress, because it is defined in terms of the actual force that acts on a body over a current area. However, it is not always possible to know a priori the configuration of a body subject to a load making Cauchy stress a difficult quantity to use in practice. A more convenient concept is the second piola-kirchoff stress tensor S which proves to be especially useful in formulating constitutive equations.

If we consider a fictitious force $\widetilde{df}$ that is defined in the reference coordinate system and acts over the oriented area NdA, formulated by mapping the actual force df in the deformed configuration:

$$\widetilde{df} = F^{-1}.df = df.F^{-T}$$

Then we can define a new traction vector and stress tensor:

$$\tilde{T}^{(N)} = \frac{\widetilde{df}}{dA} \quad \tilde{T}^{(N)} = N.S$$

Where S is the second piola-Kirchoff stress tensor.

The first piola stress tensor can be given by:

$$P = S.F^T$$

The deviatoric Cauchy stress is given by:

$$dev\ t = t - \frac{1}{3}(trt)I$$

The deviatoric stress tensor is important in modeling incompressible materials like soft tissue.

There are more ways of defining stress (Truesdell 1966) but the concepts stated above will suffice for developing models for soft tissue.

1.2.3 Balance relations

Balance relations are the field equations that must be satisfied in order for the problem to respect some fundamental laws of nature. Typically in mechanics we ensure that linear and angular momentums are conserved. (Newton's second law) Conservation of mass, conservation of energy and the law of entropy must be respected also for a natural response.

Since we will be working with isothermal formulations, we will not have to invoke the law of energy or entropy (in our field equations). However, we will ensure that momentum is conserved via field equations and ensure that mass is conserved via assumptions on the model.

The pointwise field equation that we will be solving will be:

$$\nabla . t + \rho b = \rho a$$

Where:

t is the Cauchy stress tensor

b body force vector

a is the acceleration

ρ is the material density

1.2.4 Constitutive relations

Determining the constitutive relations for biomaterials can be quite challenging. In this thesis we will be using relations given by Sacks et al. (Sacks 2000). Detailed description of these relations will follow in the section on material modeling of valves.

In general, to directly quote Humphrey (Humphrey 2001), "the five steps to formulating constitutive relations are:

1. Delineate the general characteristics of the biomaterial in question
2. Establish an appropriate theoretical framework
3. Identify specific functional form of the relation
4. Calculate values of the material parameters
5. Evaluate the predictive capability of the final relation"

1.3 SPECIFIC AIMS

The specific aims of this study are as follows:

1. To model the mechanical behavior of a healthy mitral valve
2. To calculate internal stresses as a means to predict the tension in the chordae
3. To calculate effect of altered geometry and chordal tension on coaption
4. To optimize surgical alterations so as to minimize stress induced due to surgical intervention
5. To obtain an indicator of remodeling (change in fiber direction)

2.0 METHODS

2.1 MATERIAL MODELING

Modeling the behavior of soft tissue can be a challenging undertaking in Biomechanics (Humphrey 2001) (Fung 1993). However, planar soft tissue lends itself to planar uniaxial, biaxial testing that makes it possible for us to write constitutive equations that describe fully the material behavior. (Sacks 2000)

In this thesis we will be considering both structural modeling approaches and phenomenological approaches (Sacks 2000). By structural models we mean each of its mathematical terms have physical interpretation. Adopting the structural approach gives us the ability to make inferences about the pathological states of the tissue. For instance, if we find that the tissue is more fibrous then we can increase the fiber concentration term in the constitutive relation, so on and so forth. However, sometimes it is convenient to include terms that have no direct physical interpretation, for example for modeling the rubber like behavior of the elastin matrix, Mooney -Rivlin like constitutive relations have been found useful (Fung 1993)

Before we discuss the constitutive equations, the properties of tissue that our constitutive relations must reproduce are listed below:

2.1.1 Anisotropy

Mitral valve tissue demonstrates highly anisotropic behavior. Our constitutive relations must be able to represent this anisotropy (See Figure 8). The response of the tissue is seen to be stiffer in the circumferential direction than the radial direction. This is due to the fact that tissue contains oriented fibers. Because in valve tissue the fibers tend to align in the circumferential direction, it is stiffer in response in that direction. It is very important to realize that the fiber direction in mitral valve tissue is only the mean direction of a collection of fibers. We use the circumferential and radial coordinate system because of the shape of the mitral valve leaflet. See Figure 7

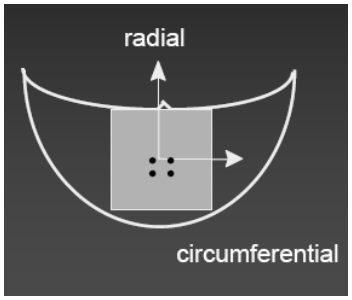

Figure 7: Circumferential and radial direction of patch of material in mitral valve leaflet

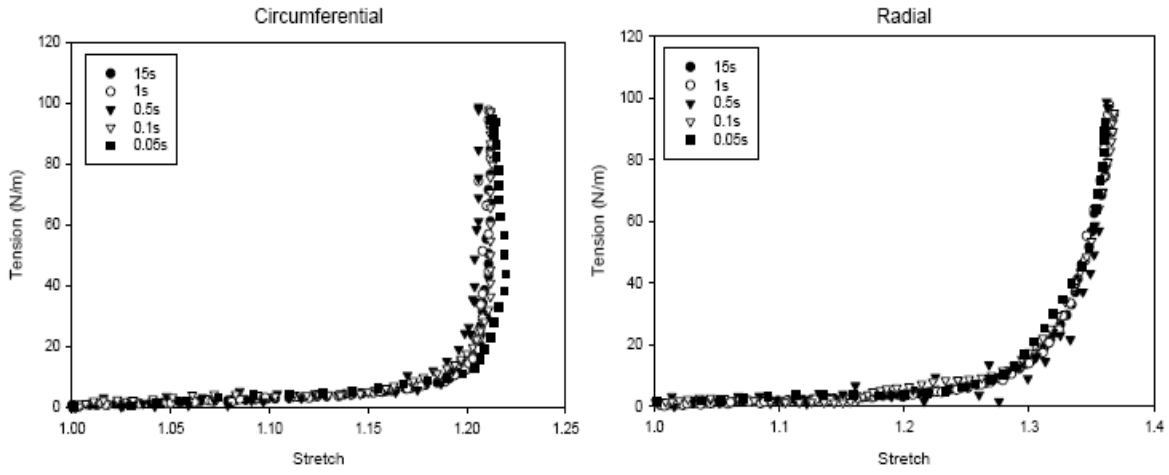

Figure 8: Mitral valve tissue exhibits different response in circumferential directions

Source: (Liao 2007)

Liao et al. suggest that the mitral valves are strain rate insensitive in the physiologic loading range. They performed biaxial tests where they loaded the specimen to same levels of load in 0.05 s to 15 s and saw no significant change in the stress strain curve as shown in Figure 8. Thus strain rate effects are not considered herein.

2.1.2 Fiber un-crimping

Aside from the fact that the tissue response is different between the radial and circumferential direction, Figure 8 illustrates a typical property of soft tissue: the extended toe region of the stress/strain curve. This occurs because the collagen fibers in the tissue are crimped. Our constitutive relations will have to take this fact into account. Depending on how crimped a collagen is, the toe region characteristics are different in different tissues. Our constitutive model also has to capture the un-crimping dynamics of the collagen fibers. Figure 9 shows collagen crimp in tissue visible under a microscope.

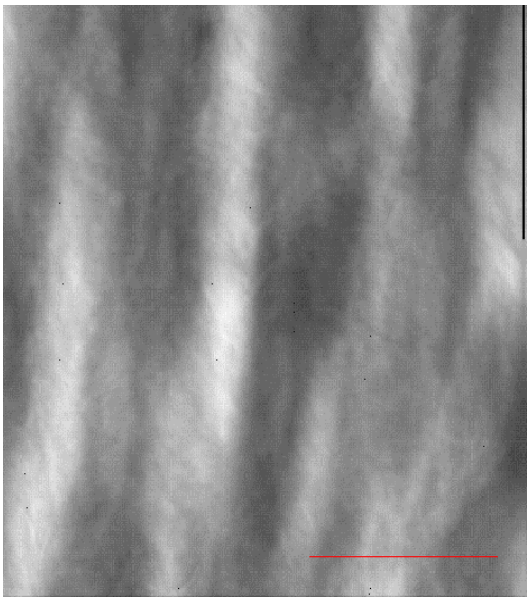

Figure 9: Collagen crimp (Billiar and Sacks 1997)

2.1.3 Fiber rotation

Because the fiber is embedded in the tissue, it rotates as well as stretches as the tissue deforms. Because the fibers rotate, some interesting mechanical effects emerge, which can well be represented by the Chinese fan model as shown in Figure 11. The fibers align in the geometric configuration that gives the tissue a stiffer response. Figure 10 illustrates the effect in terms of stress strain curves. The tissue exhibits a hardening behavior as stretch increases. This is a reflection of the fact that as the tissue is stretched more fibers line up and thus the overall stiffness of the tissue is increased.

It is important to note that this re-orientation is at a scale larger than the material point in our continuum approximation. If we consider an infinitesimal patch (element) on the planar tissue, then within that element we can calculate the mean fiber direction. This is the mean direction of orientation of all the collagen fibrils within that element. Now, The material may deform such that the fiber direction of each element alligns making the overall stiffness of the material in that direction appear elevated. This apparent stiffening of the material with increased strain can be captured by correctly modeling fiber directions in the elements, as well as the uncrimping of the fibers.

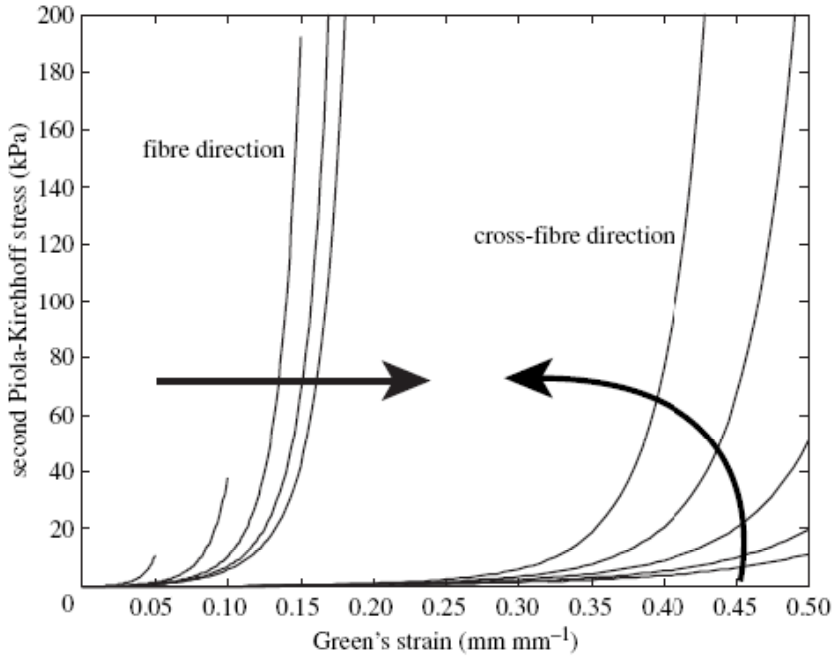

Figure 10: Increase in stiffness with increase in stretch, source: (K. Kunzelman 2007)

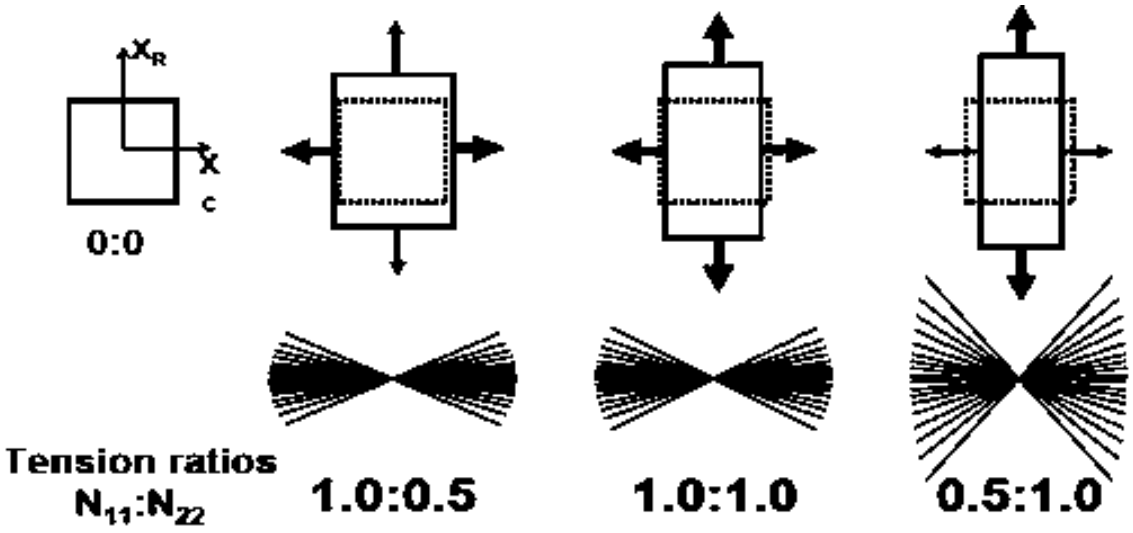

Figure 11: Fiber reorientation with stretch. Different stretches produce different reorientation.

2.1.4 Fiber splay

Fiber splay models the distribution of the fibers around the mean fiber direction at a single material point. In valve tissue the fiber direction includes a mean direction of a collection of fibers, as well as the distribution of the fibers about this mean direction. This distribution about the mean might also change with stretch or tension (see Figure 13)

SALS (Cochran 1991) study shows that certain regions, typically the belly sections, of the mitral valve have highly aligned collagen fibers while other sections have dispersed fibers. (Sacks 2000). Taking the initial heterogeneity of alignment into consideration is extremely important if we are to accurately predict the stress and strain in mitral valve. Fortunately, fiber orientation maps can be obtained from tissue samples. Figure 12 shows one such map. The lines indicate the mean fiber orientation and the darkness of color indicates if the fiber distribution about the mean is tight.

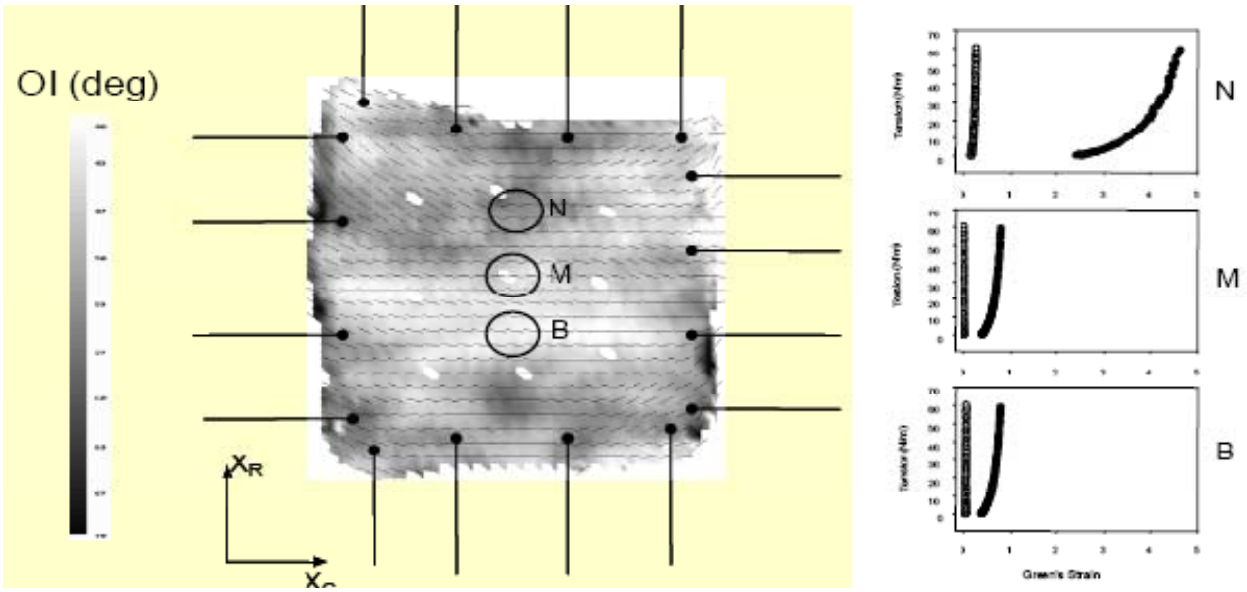

Figure 12: Sections N, M and B have different response, source: (Sacks 2000)

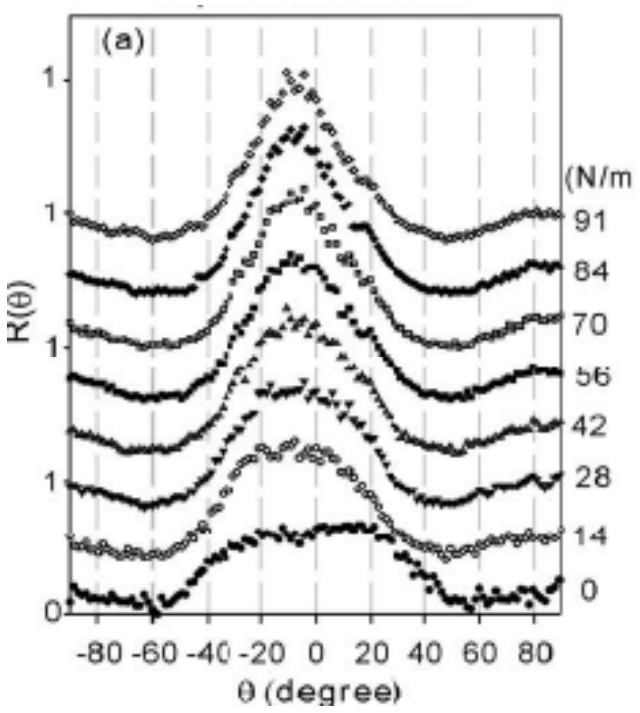

Figure 13: Change in fiber splay under equi-biaxial stretch, source: (Liao 2007)

The change in fiber splay with stretch is not very well understood. Therefore, to take the fiber splay into account we only model the mean fiber direction in an isotropic matrix and define the distribution about the mean via statistical parameters. This representation gives us sufficient accuracy to make inferences about surgical procedures effects on the valve (Dal 2005).

2.2 CONSTITUTIVE EQUATIONS

As explained in the previous section, the material response of the mitral valve is a complex in part because of the collective response of oriented fibers in an isotropic matrix. It is not possible to represent every fibril and it's direction, however the mean fiber direction within an infinitesimal area element can be obtained by SALS experiments (Cochran 1991). It is also possible to obtain the distribution of the fibers that constitute the tissue about their mean fiber direction (Cochran 1991). The distribution is modeled statistically, while the mean is modeled as a preferred material direction. Here we chose a transverse isotropic material model to represent our tissue.

Transverse isotropy (weiss 1996) is a class of symmetry wherein the stress at a material point depends both on the deformation gradient and a fiber orientation. In our case the fiber orientation is going to be the mean fiber direction of all the collagen fibers in the matrix.

Weiss et al. presented a formulation for modeling soft tissue (weiss 1996)which we followed closely for the present model development. We will depart from their formulation by adding the required terms to model fiber splay (Sacks 2000). Our approach is similar to Einstein et al. (Einstein 2002) except that their group chose to implement shell elements wheras we chose to represent the material with solid elements for their ability to better impose incompressibility conditions.

To enforce transverse isotropy we have two options:

1. Specify the way in which the strain energy depends on the deformation (Green 1970)
2. Introduce a vector to represent the material preferred direction (Spencer 1984)

A combination of the two approaches is followed herein. Spencer's (Spencer 1984) original vector derivation is presented below with modification for clarity. Consider a^0 to be a unit vector representing the mean fiber direction in the un-deformed configuration. We will require that the strain energy depend on this vector.

We assume a 'affine' deformation. That is to say that vector field $a^0(X)$ will deform with the material. Let λ denote the fiber stretch.

Denoting the deformation gradient, F, let the unit vector in the un-deformed and deformed configurations be a^0 and a, respectively, then the fiber stretch gives,

$$\lambda a = F.a^0$$

Since a is a unit vector, the following holds true also:

$$\lambda^2 aa = \lambda^2 = a^0.F^T F.a^0 = a^0.C.a^0$$

At this point we are going to assume that the material is hyperelastic (Humphrey 2001). Such an assumption is valid when the tissue reaches a preconditioned state (Humphrey 2001). Under the hyperelastic assumption we can define a strain energy density function W that represents the stored energy at material point x, the derivative of which with respect to strain gives the stress at that point. The strain energy function W, represents the stored energy so it must obey the principle of material frame indifference (Spencer 1984). The strain energy function must also be a function of the right Cauchy deformation gradient (from elasticity) and because of our transverse isotropy assumption it must also be a function of the tensor product $a^0 \otimes a^0$.

Therefore W can be expressed as:

$$W(X, C, a^0) = W(X, QCQ^T, Qa^0 \otimes a^0 Q^T) \ \forall \ (C, Q)$$

Where:

$Q$is any transformation on $C\ or\ a^0$ (for material frame indifference)

Spencer further showed that when W is an isotropic function of C and $a^0 \otimes a^0$ then five invariants are sufficient to describe the relation fully (Spencer 1984). They are:

$$I_1 = tr\ C$$

$$I_2 = \frac{1}{2}[(tr\ C)^2 - tr\ C^2]$$

$$I_3 = \det C = J^2$$

$$I_4 = a^0.C.a^0$$

$$I_5 = a^0.C^2.a^0$$

I_1, I_2, I_3 are the standard strain invariants associated with isotropic behavior while I_4, I_5 arise from the anisotropy introduced by the fiber distribution. The strain energy function can now be represented as:

$$W(X, C, a^0) = W(X, I_1(C), I_2(C), I_3(C), I_4(C, a^0), I_5(C, a^0))$$

Having chosen this form we are assured the satisfaction of material frame indifference and transverse isotropy. The stress and elasticity tensors remain to be developed based on this form of W.

2.2.1 Stress tensor

The second Piola Kirchhoff stress tensor is derived from the strain energy density function (by definition of hyperelastic material) (Fung 1993)

$$S = 2\frac{\partial W}{\partial C}$$

Since, $W(X, C, a^0) = W(X, I_1(C), I_2(C), I_3(C), I_4(C, a^0), I_5(C, a^0))$ we can write S in terms of the invariants:

$$S = 2\sum_{\alpha=1}^{5}\left(\frac{\partial W}{\partial I_\alpha}\frac{\partial I_\alpha}{\partial C}\right)$$

where,

$$\frac{\partial I_1}{\partial C} = 1$$

$$\frac{\partial I_2}{\partial C} = I_1\,\mathbb{I} - C$$

$$\frac{\partial I_3}{\partial C} = I_2\,\mathbb{I} - I_1 C + C^2 = I_3 C^{-1}$$

$$\frac{\partial I_4}{\partial C} = a^0 \otimes a^0$$

$$\frac{\partial I_5}{\partial C} = a^0 \otimes C.a^0 + a^0.C \otimes a^0$$

Because soft tissue is considered to be an incompressible material (Humphrey 2001), the third invariant becomes a constant, $I_3 = \det C = J^2 = 1$. Thus the strain energy density function can be given as a function of $only\ I_1, I_2, I_4\ and\ I_5$. A lagrange multiplier p is used to enforce the condition of incompressibility.

The second Piola-Kirchhoff stress tensor can now be given as:

$$S = 2\{(W_1 + I_1 W_2)\mathbb{I} - W_2 C + W_4 a^0 \otimes a^0 + W_5(a^0 \otimes C.a^0 + a^0.C \otimes a^0)\} + pC^{-1}$$

Where:

$$W_a = \frac{\partial W}{\partial I_a} \text{ and } \mathbb{I} = \delta ij$$

The Cauchy stress can readily be derived from S as follows,

$$(\sigma)_{ij} = \frac{1}{J} F_{iI} F_{jJ} S_{IJ}$$

$$= 2\{(W_1 + I_1 W_2)B - W_2 B^2 + I_4 W_4 \, a \otimes a + I_4 W_5 (a \otimes B.a + a.B \otimes a)\} + p$$

Where:

B is left green tensor, $\mathbb{I} = \delta ij$.

This completes the derivation of the stress tensors. Next, we give the closed form expressions for elasticity tensors for our material model. These were originally derived by Weiss et al. (weiss 1996) and are included for completeness.

2.2.2 Elasticity tensor

The second elasticity tensor in its material form is given as:

$$C := 4 \frac{\partial^2 W}{\partial C \, \partial C} = 2 \frac{\partial S}{\partial C}$$

Since $S = 2\{(W_1 + I_1 W_2)\mathbb{I} - W_2 C + W_4 a^0 \otimes a^0 + W_5 (a^0 \otimes C.a^0 + a^0.C \otimes a^0)\} + pC^{-1}$

A direct substitution gives,

$$C = 4\left\{\mathbb{I} \otimes \frac{\partial W_1}{\partial C} + \mathbb{I} \otimes W_2 \frac{\partial I_1}{\partial C} + \mathbb{I} \otimes I_1 \frac{\partial W_2}{\partial C} - W_2 \frac{\partial C}{\partial C} + a^0 \otimes a^0 \otimes \frac{\partial W_4}{\partial C} + \frac{\partial I_5}{\partial C} \otimes \frac{\partial W_5}{\partial C} + W_5 \frac{\partial^2 I_5}{\partial C \partial C}\right\} + pI_{c-1}$$

Where:

I_{c-1} is the derivative $\frac{\partial C^{-1}}{\partial C}$ (this term is as left as is since the derivative disappears in the spatial version)

Weiss et al. gave the closed form expressions for the second elasticity tensor after further application of the chain rule and some more manipulation as follows,

$$\mathrm{C} = 4\left\{\begin{array}{c}(W_{11} + 2W_{12}I_1 + W_2 + W_{22}I_1^2)\mathbb{I}\otimes\mathbb{I} \\ -(W_{12} + W_{22}I_1)(\mathbb{I}\otimes C + C\otimes\mathbb{I}) + W_{22}(C\otimes C) - W_2 I \\ +(W_{14} + W_{24}I_1)(\mathbb{I}\otimes a^0\otimes a^0 + a^0\otimes a^0\otimes\mathbb{I}) + W_5\dfrac{\partial^2 I_5}{\partial C\partial C} \\ +(W_{15} + W_{25}I_1)\left(\mathbb{I}\otimes\dfrac{\partial I_5}{\partial C} + \dfrac{\partial I_5}{\partial C}\otimes\mathbb{I}\right) \\ -W_{24}(C\otimes a^0\otimes a^0 + a^0\otimes a^0\otimes C) - W_{25}\left(C\otimes\dfrac{\partial I_5}{\partial C} + \dfrac{\partial I_5}{\partial C}\otimes C\right) \\ +W_{44}(a^0\otimes a^0\otimes a^0\otimes a^0) + W_{45}(a^0\otimes a^0\otimes\dfrac{\partial I_5}{\partial C} + \dfrac{\partial I_5}{\partial C}\otimes a^0\otimes a^0) \\ +W_{55}(\dfrac{\partial I_5}{\partial C}\otimes\dfrac{\partial I_5}{\partial C})\end{array}\right\} + pI_{c-1}$$

Where: $W_{ab} = \frac{\partial^2 W}{\partial a\partial b}$

The spatial version of the elasticity tensor can be found in in (weiss 1996)

2.2.3 Special Considerations for incompressible materials

Incompressible materials are susceptible to numerical inaccuracy if traditional (pure displacement) finite element procedures are used to solve the balance equations. The most common of these problems are volume locking and shear locking. Volume locking, as the name suggests has to do with the dilatation portions of the deformation gradient tensor while shear locking occurs in the deviatoric portion (Sussman 1987).

In order to alleviate this problem we will choose separate numerical treatment for the dilatation and deviatoric parts. We will therefore seek a multiplicative split the deformation

gradient of the dilatation and deviatoric portion, $F_{vol}\ and\ \tilde{F}, respectively$, as given by Simo (Simo 1985):

$$F = F_{vol}\tilde{F}$$

$$F_{vol} := J^{1/3}\mathbb{I}$$

$$\tilde{F} := J^{-1/3}F$$

Where:

$\det F_{vol} = J\ \ and \det \tilde{F} = 1$

Accordingly, the right Cauchy-Green deformation tensor can be given in terms of J and $\tilde{F}$ as:

$$C = F^T F = J^{\frac{2}{3}}\tilde{C}$$

$$where\ \tilde{C} = \tilde{F}^T\tilde{F}$$

We will also, uncouple the strain energy function (Simo 1985)in terms of the dilatation and deviatoric components, such that:

$$W = U(J) + \widetilde{W}(\tilde{C})$$

With this form of strain energy function chosen, the second Piola-Kirchhoff stress tensor can be obtained as:

$$S = pJC^{-1} + 2J^{-2/3}Dev\left[\frac{\partial \widetilde{W}}{\partial \tilde{C}}\right]$$

Again we can calculate the Cauchy stress as:

$$\sigma = p1 + \frac{2}{J}Dev\left[F\frac{\partial \widetilde{W}}{\partial \tilde{C}}F^T\right]$$

In their uncoupled form:

$$I_1 = tr\ \tilde{C} = J^{\frac{-2}{3}}trC$$

$$I_2 = \frac{1}{2}\left[\left(tr\,\tilde{C}\right)^2 - tr\,\tilde{C}^2\right] = \frac{J^{-\frac{4}{3}}}{2}((trC)^2 - trC^2)$$

$$I_4 = a^0.\tilde{C}.a^0 = J^{\frac{-2}{3}}a^0.C.a^0$$

$$W = U(J) + \widetilde{W}\left(\tilde{C}\right) = \widetilde{F_1}(I_1, I_2) + \widetilde{F_2}(I_4) + \widetilde{F_3}(I_1, I_2, I_4) + U(J)$$

$$\frac{\partial \widetilde{W}}{\partial \tilde{C}} = \left(\widetilde{W_1} + \widetilde{W_2}\tilde{I_1}\right)\mathbb{I} - \widetilde{W_2}\tilde{C} + \widetilde{W_4}a^0 \otimes a^0$$

$$Dev\left[\frac{\partial \widetilde{W}}{\partial \tilde{C}}\right] = \left(\widetilde{W_1} + \widetilde{W_2}\tilde{I_1}\right)\mathbb{I} - \widetilde{W_2}\tilde{C} + \widetilde{W_4}a^0 \otimes a^0 - \frac{1}{3}\left(\widetilde{W_1}\tilde{I_1} + 2\widetilde{W_2}\tilde{I_2} + \widetilde{W_4}\tilde{I_4}\right)\tilde{C}^{-1}$$

$$S = pJC^{-1} + 2J^{-\frac{2}{3}}\left[\left(\widetilde{W_1} + \widetilde{W_2}\tilde{I_1}\right)\mathbb{I} - \widetilde{W_2}\tilde{C} + \widetilde{W_4}a^0 \otimes a^0 - \frac{1}{3}\left(\widetilde{W_1}\tilde{I_1} + 2\widetilde{W_2}\tilde{I_2} + \widetilde{W_4}\tilde{I_4}\right)\tilde{C}^{-1}\right]$$

$$F\frac{\partial \widetilde{W}}{\partial \tilde{C}}F^T = \left(\widetilde{W_1} + \widetilde{W_2}\tilde{I_1}\right)\tilde{B} - \widetilde{W_2}\tilde{B}^2 + \widetilde{W_4}\tilde{I_4}a^0 \otimes a^0$$

$$\sigma = p1 + \left(\widetilde{W_1} + \widetilde{W_2}\tilde{I_1}\right)\tilde{B} - \widetilde{W_2}\tilde{B}^2 + \widetilde{W_4}\tilde{I_4}a^0 \otimes a^0 - \frac{1}{3}\left(\widetilde{W_1}\tilde{I_1} + 2\widetilde{W_2}\tilde{I_2} + \widetilde{W_4}\tilde{I_4}\right)\tilde{C}^{-1}$$

$$c = p(\mathbb{I} \otimes \mathbb{I} - 2I) - \frac{2}{3}(dev\,\sigma \otimes \mathbb{I} + \mathbb{I} \otimes dev\,\sigma) + \frac{4}{3J}\left(\frac{\partial \widetilde{W}}{\partial \tilde{C}} : \tilde{C}\right)\left[I - \frac{1}{3}(\mathbb{I} \otimes \mathbb{I})\right] + \tilde{c}_{\widetilde{w}}$$

Where:

$$\tilde{c}_{\widetilde{W}} is\ the\ push\ forward\ of\ \tilde{C}_{\widetilde{W}} = \frac{\partial^2 \widetilde{W}}{\partial \tilde{C}\partial \tilde{C}}$$

$$\mathbb{I} = \delta_{ij}$$

The above equations were first obtained by Weiss et al (weiss 1996).

Note that the 5th Invariant $I_5 = a^0.C^2.a^0$ was dropped from the formulation in the uncoupled form. This was essentially to simplify implementation but also since I_4 already depends on the fiber direction, in our structural constitutive equation it is sufficient for $\widetilde{W}$ to be a function of I_1, I_2, I_4

2.2.4 Choice of a form for $\widetilde{W}$

A functional form for $\widetilde{W}$ remains to be chosen (Humphrey 2001). Since we have assumed tissue will be represented by collagen fibers in an isotropic matrix, we will chose a form for $\widetilde{W}$ given by:

$$\widetilde{W} = \widetilde{F_1}(I_1, I_2) + \widetilde{F_2}(I_4) + \widetilde{F_3}(I_1, I_2, I_4)$$

Where :

$\widetilde{F_1}(I_1, I_2)$ is the contribution due to the isotropic matrix

$\widetilde{F_2}(I_4)$ is the contribution due to orientation

$\widetilde{F_3}(I_1, I_2, I_4)$ is the contribution due to the coupling of matrix and fiber

The choice of $\widetilde{F_1}(I_1, I_2)$ is standard:

$$\widetilde{F_1}(I_1, I_2) = c_1(I_1 - 3) + c_2(I_2 - 3)$$

Where:

c_1, c_2 are material constants

$I_1 = tr\ C$

$I_2 = \frac{1}{2}[(tr\ C)^2 - tr\ C^2]$

Representing isotropic behavior of elastomers by two invariants in this way is common (Spencer 1984) The choice of $\widetilde{F_2}(I_4)$is more critical. Since most of the strain energy is stored in the crimped collagen fibers. Also, $as\ I_4 = \lambda$, $\widetilde{F_2}(I_4) = \widetilde{F_2}(\lambda)$, λ is the stretch in the fiber direction. $\widetilde{F_2}(\lambda)$ is chosen as follows,

$$\frac{d\widetilde{F_2}(\lambda)}{d\lambda} = A\left[exp\left[\frac{B}{2}(\lambda - 1)\right] - 1\right]$$

Where:

A and B are material parameters

A represents the volume fraction of collagen

B is the stiffness of the equivalent fiber

The underlying reason for using an exponential form of $\widetilde{dF_2}(\lambda)/_{d\lambda}$ is that it captures the fiber recruiting (namely, stretching of fiber one after another) and the fiber uncrimping phenomenon that is prevalent in tissue (Humphrey 2001).

The form of $\widetilde{F_3}(I_1, I_2, I_4)$ is difficult to guess apriori; moreover, shear experiments are difficult thus so source of calibration is not available yet. As a result, this form ends up not used at this time.

One alternative is to assume a Fung type $\widetilde{W}$ with shear terms retained and then fit to experimental data:

$$\widetilde{W} = \frac{c}{2}[exp(A_1E_{11}^2 + A_2E_{22}^2 + 2A_3E_{11}E_{22} + A_4E_{12}^2 + 2A_5E_{11}E_{12} + 2A_6E_{22}E_{12}) - 1]$$

This indeed provides some shear coupling, but this is a phenomenological model and the constants don't have physical meaning associated to them. The employment of this model would not allow the later study of tracing the physical factors that lead to a change in stress state. So, this form is not desirable either.

We therefore also neglect the $\widetilde{F_3}(I_1, I_2, I_4)$ term in our approximation. Instead we use an alternative approach in which we introduce a statistical measure for fiber distribution about the mean orientation. The mooney rivlin coefficients in our model then stand for the stiffness of the overall isotropic response of the tissue. The shear terms that occur in our formulation are from the isotropic portion of the formulation.

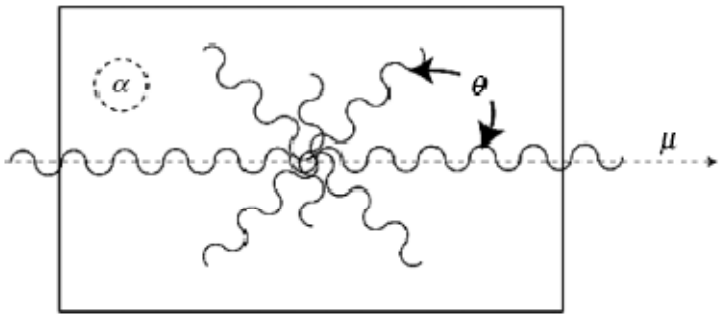

Figure 14: Collagen fibers are distributed in plane, source: (K. Kunzelman 2007)

To capture the statistical distribution of the collagen fiber in the plane of the tissue, Sacks et al. introduced the normally distributed parameter $R(\theta)$

$$R(\theta) = \frac{1}{\sigma\sqrt{2\pi}} exp\left[\frac{-(\theta - M)^2}{2\sigma^2}\right]$$

Where:

M is the mean fiber direction

θ is the deviation from the mean direction

σ is the variance of the normal distribution

The strain energy contribution in the mean fiber direction is now due to an integrated response of the fibers normally distributed about the mean. To incorporate this fact we make the following changes:

$$\lambda = T(\theta).C.T(\theta)$$

Where:

$T(\theta)$ is the rotation tensor of a fiber orientated at angle θ from mean direction

We can denote $\frac{d\widetilde{F_2}(\lambda)}{d\lambda}$ by sf (stress in fiber direction) for ease of representation.

$$sf = \frac{d\widetilde{F_2}(\lambda)}{d\lambda} = A\left[exp\left[\frac{B}{2}(T(\theta).C.T(\theta) - 1)\right] - 1\right]$$

The contribution of all the fibers together is now:

$$\widetilde{W_4} = \int_{-\pi/2}^{\pi/2} sf \,.\, R(\theta)\, d\theta$$

We assume that the strain energy of all fibers distributed about the mean is the summation of each fiber stretch along its axis

Thus $\frac{\partial \widetilde{W}}{\partial \tilde{C}}$ can now be written explicitly as:

$$\frac{\partial \widetilde{W}}{\partial \tilde{C}} = \left(\widetilde{W_1} + \widetilde{W_2}\tilde{I_1}\right)1 - \widetilde{W_2}\tilde{C} + \widetilde{W_4} a^0 \otimes a^0$$

Where;

$\widetilde{W_4} = \int_{-\pi/2}^{\pi/2} sf \,.\, R(\theta)\, d\theta$

The second Piola Kirchhoff stress tensor and the Cauchy stress tensor can now be calculated based on the equations given in the previous section.

2.2.5 Implementation

We only need to evaluate the integral term of $\frac{\partial \widetilde{W}}{\partial \tilde{C}}$ and implement it in LSDYNA via a subroutine to LSDYNA called USERMAT.

To evaluate the integral term Einstein et al. (Einstein 2002) used the trapezoidal rule, considering 18 equal divisions of 10 degrees each. Adopting this, we evaluate the discreet form of the integral term:

$$\widetilde{W_4} = \frac{A\pi}{18\sigma\sqrt{\pi}}\left[\sum_{k=1}^{17} \exp\left[\frac{B}{2}(I_4(\Phi)\right] - 1\right]\Xi(\Phi)$$

Where:

is the integral portion of $\frac{\partial \widetilde{W}}{\partial \tilde{C}}$

$$\Phi = \left[-\frac{1}{2}\pi + \frac{1}{18}k\pi\right]$$

$$\Xi = exp\left(-\frac{1}{2}\frac{(\Phi-\mu)^2}{\sigma^2}\right)$$

$$I_4 = T(\Phi).\tilde{C}.T(\Phi)$$

$$T = \begin{bmatrix} \cos^2\Phi & \sin\Phi\cos\Phi & 0 \\ \sin\Phi\cos\Phi & \sin^2\Phi & 0 \\ 0 & 0 & 0 \end{bmatrix}$$

2.3 VALIDATION

The material model that we developed and implemented in LSDYNA now needs to be validated against experimental data, and the material parameters need to be fitted to available data so that the stress strain curves obtained from our model match experimentally measured values as closely as possible. In order to achieve this end we used a pre-packaged optimization tool LS-OPT (lsopt 2008). The parameter estimation capability of LS-OPT works on a history based Mean square error principle, i.e. it minimizes the mean square error between the simulation results and the experimental results. The material parameters that provide the least error are reported.

Newman and Yin (May-Newman 1998) performed biaxial stretching of mitral valve tissues under several protocols. Their equibiaxial stretch data were used to estimate parameters for our model.

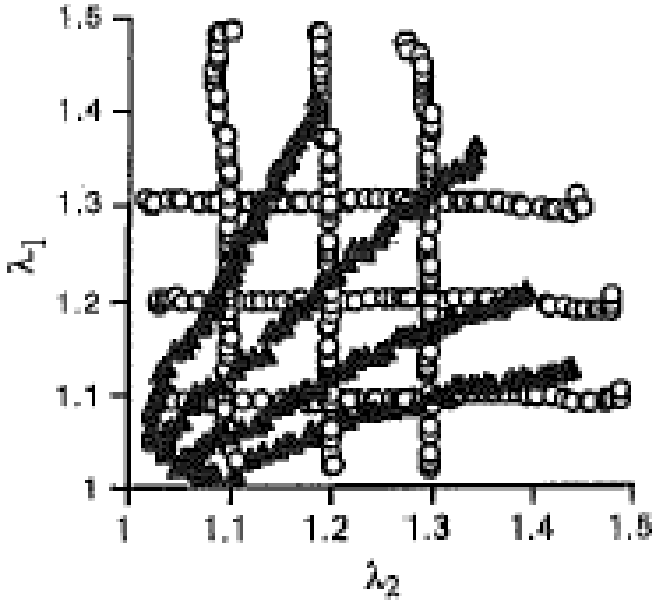

Figure 15: Various protocols for biaxial stretch, source: (May-Newman 1998)

For our validation study, a computational model of the equibiaxial stretch test was prepared. Because of symmetry, only a quarter of the sample is modeled as a 1cmx1cm patch in ANSYS. The patch was further divided into 25 elements. Displacements were specified at all the nodes on the top and right edges, namely at x=1 and y =1, respectively. . At x=0 or y=0 the symmetry condition is imposed as illustrated in Figure 16

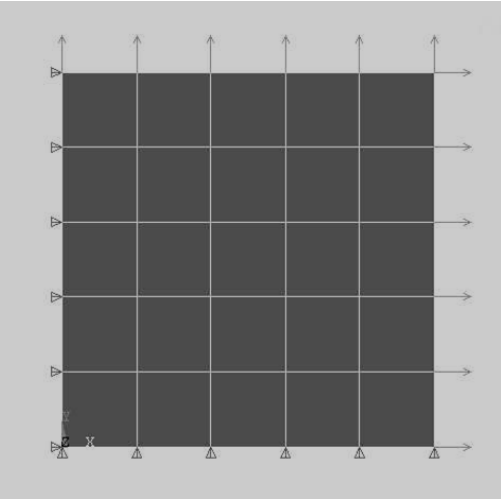

Figure 16: Model of equibiaxial test

Further, the fiber angle in the elements was changed from 0 to 45 degrees and the biaxial test was repeated. The shear stress in plane was calculated and compared with the experimental results obtained by Hyunggun et al. (HYUNGGUN, et al. 2007)

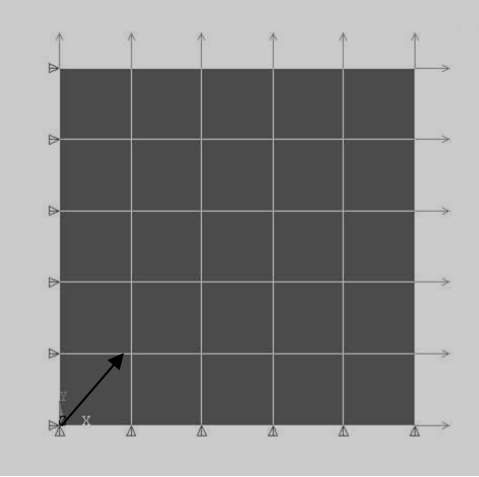

Figure 17: Fiber angle 45 degrees

Model parameters were fit till the minimum error was obtained, and the stress-strain curves for the center element are plotted herein to illustrate the fit.

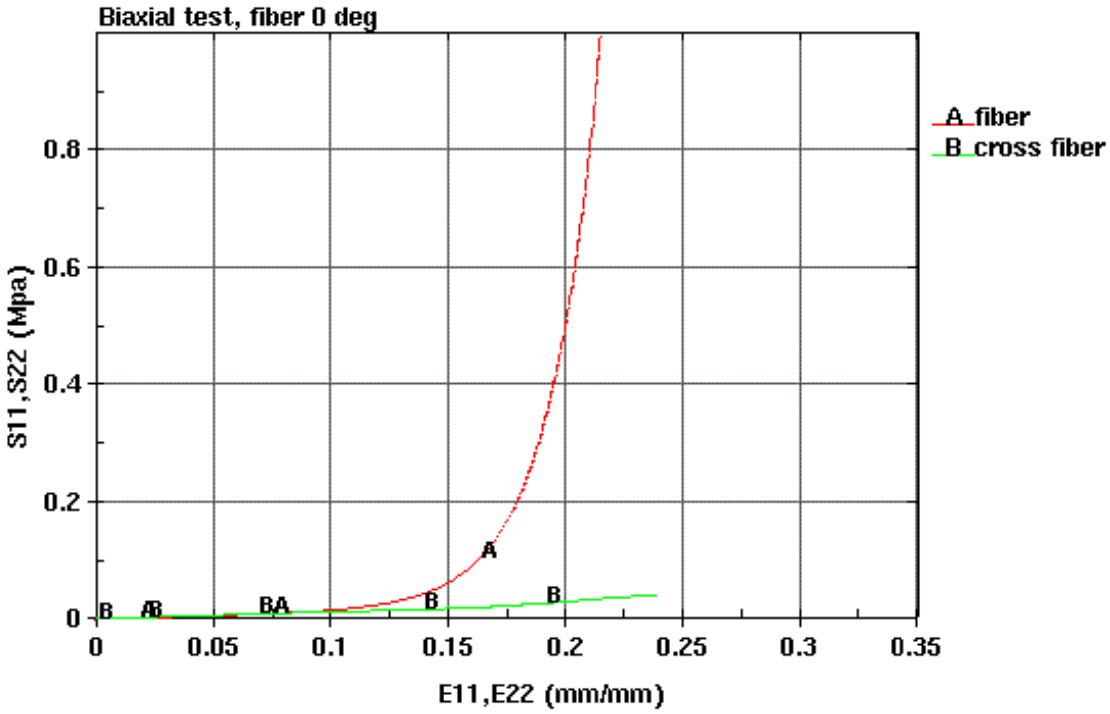

Figure 18: Stress strain curve for Anterior leaflet

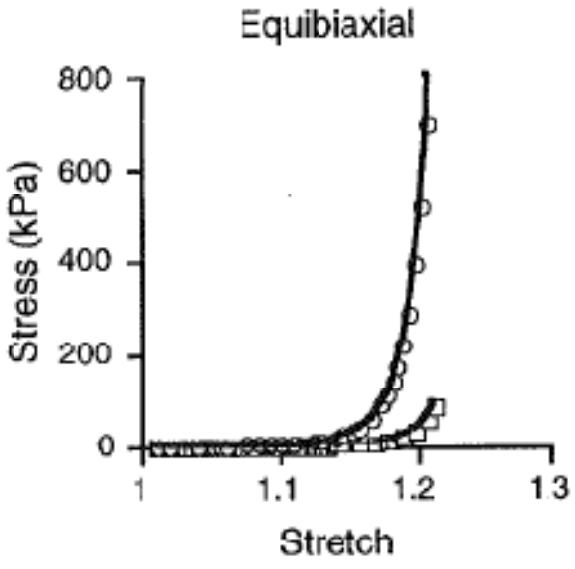

Figure 19: Experimentally measured stress strain curve Anterior leaflet, source: (May-Newman 1998)

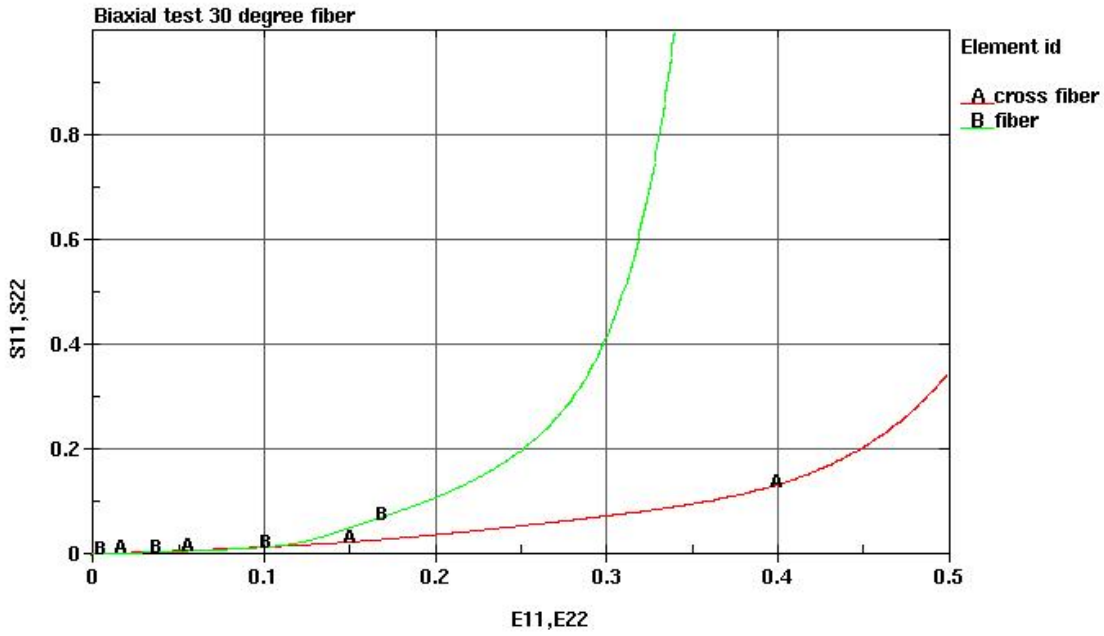

Figure 20: Stress strain plots when fiber angle is rotated to 30 degrees

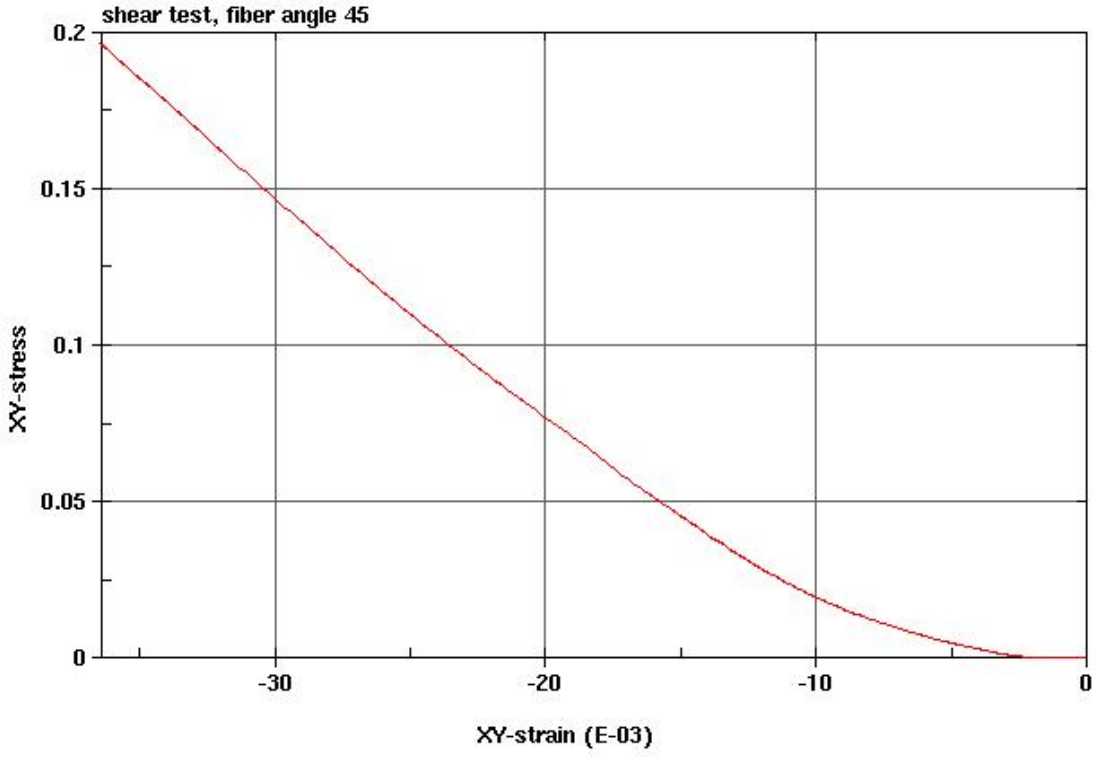

Figure 21: Shear stress in biaxial test with fiber angle at 45 degrees

Note that the shear experiment data are available for chemically treated valve tissue only. So the data is for comparison of trend only.

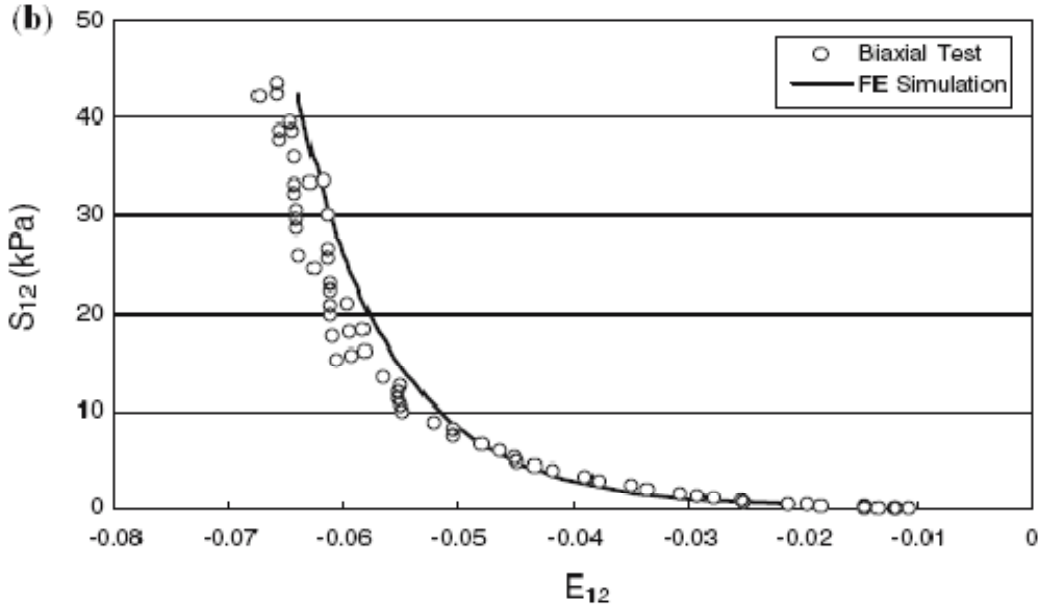

Figure 22: Shear test data, source: (HYUNGGUN, et al. 2007)

The stress strain curves show good agreement with the experimental data. The parameters for our model are thus reported below:

Table 1: Material parameters for Mitral valve tissue

Material parameter	value
A	0.07
B	40e-3 Mpa
C1	0.65e-2
C2	0.1e-2
σ	20

2.4 GEOMETRIC MODELING

2.4.1 Annulus Shape

Prot et al. (Prot 2007) conducted echocardiography experiments on a pig (hybrid: Duroc, Yorkshire, Landsvin) and then excised the mitral valve for anatomical measurements postmortem. Their experiments were the primary source for the geometric quantities of our mitral valve model

The shape of the annulus was considered to be approximately elliptical (see Figure 23). The leaflet lengths and curvature were derived from published echocardiography data shown in Figure 24. The anterior leaflet was assumed to have a smaller annular length and that the annular attachment is almost straight. The posterior leaflet is assumed to occupy the rest of the annular length which is much more curved. The saddle height (see Figure 23) reported in (Prot 2007) was ignored for the time being because the author reported no significant change in results due to the inclusion of this parameter.

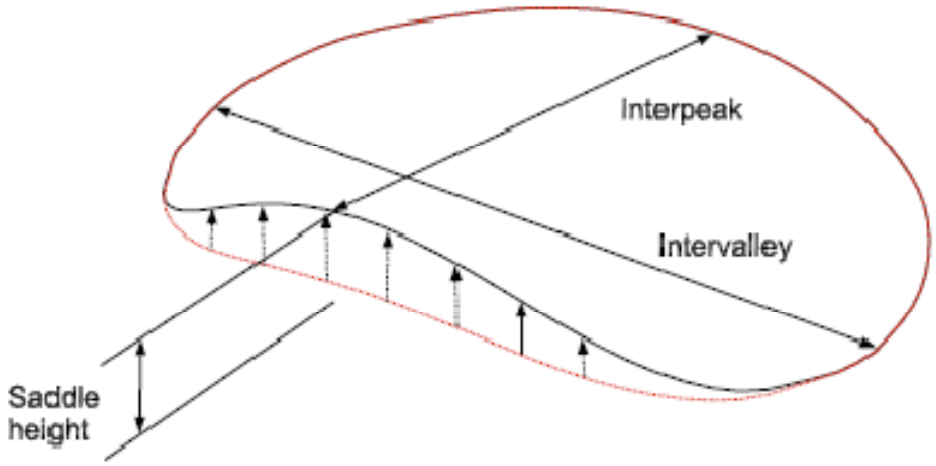

Figure 23: Shape of mitral annulus and leaflets, Source: (Prot 2007)

Table 2: Variation in geometric properties through systole, source: (Prot 2007)

	Saddle height (mm)	Intervalley (mm)	Interpeak (mm)	Perimeter (mm)
Beginning of systole	4.81	34.1	30.9	103.5
Peak Systole	6.85	35.6	31.4	108.5

Changes in intervalley distance, interpeak distance, perimeter as reported by prot et. al. were very small. Therefore these values remain constant in our model: they remain at the levels at the beginning of systole in our model.

2.4.2 Leaflet Height

The leaflet height and curvature were estimated from echocardiography data (see Figure 24)

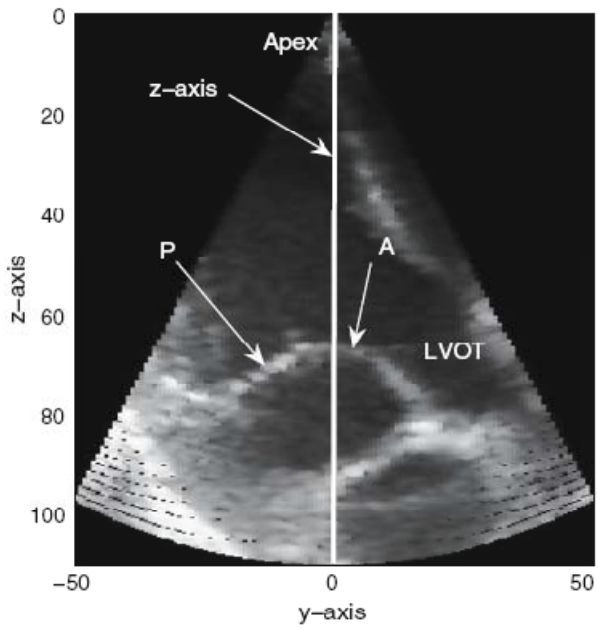

Figure 24: Echocardiograph showing leaflet height and curvature, source: (Prot 2007)

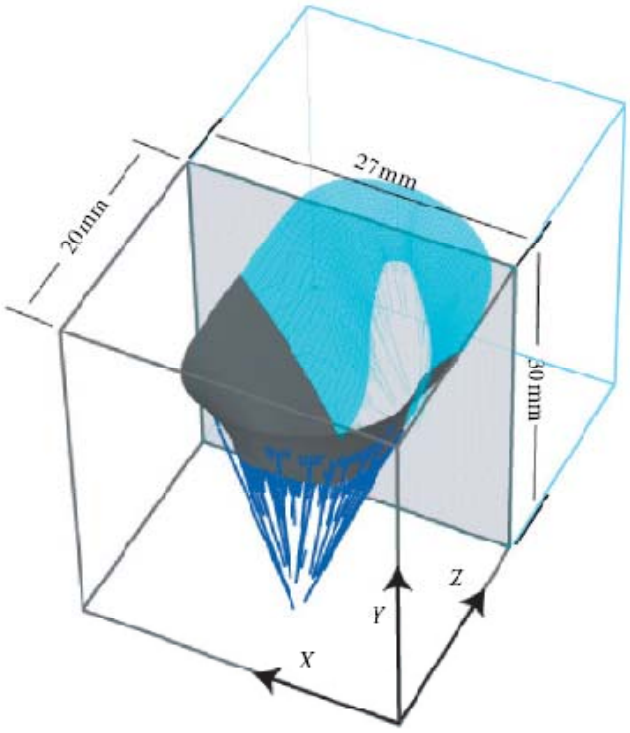

Figure 25: Gross dimensions of FE model, source: (K. Kunzelman 2007)

Based on the above reported parameters, a three dimensional shape was created in the commercial computer aided modeling software SOLIDWORKS and then imported into ANSYS for processing. In ANSYS the mid-surface through thickness of the geometry was extracted. The extraction of the midsurface allows us to make a shell approximation as well as gives us the ability to extrude a mesh perpendicular to the midsurface for a solid approximation.

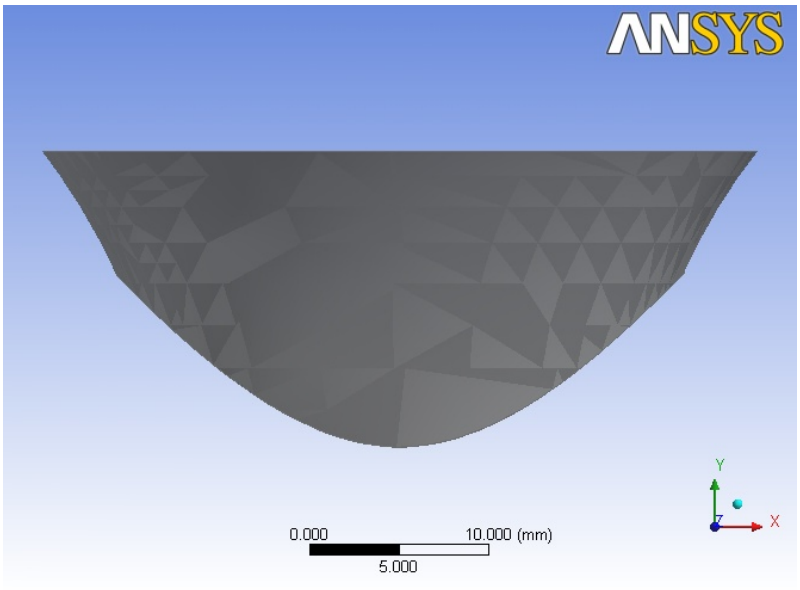

Figure 26: The mitral valve solid model (front)

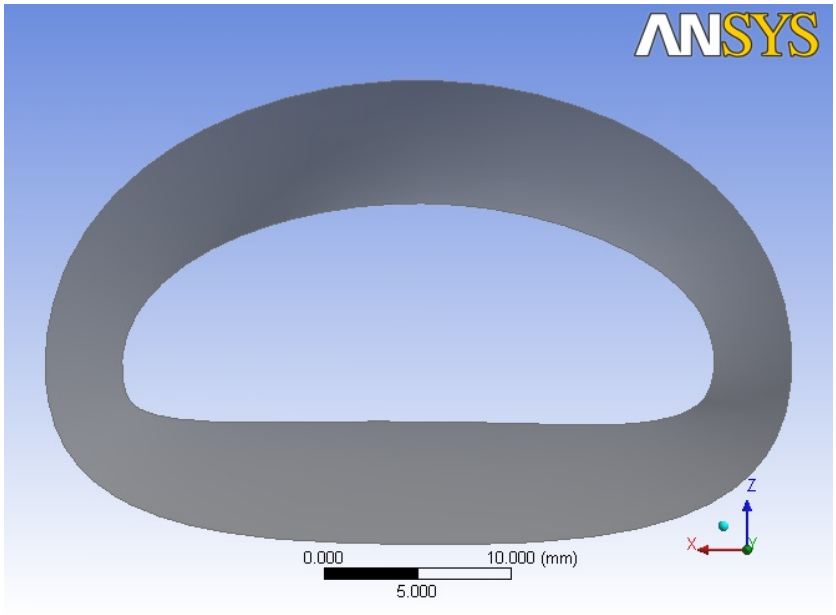

Figure 27: The mitral valve solid model (Top)

2.4.3 Modeling the Chordae: Position and distribution

Bajona et al. (Bajona 2008). excised fresh porcine mitral valves for measurement of tension in the chordae in a pressure-flow simulator see Figure 28 below.

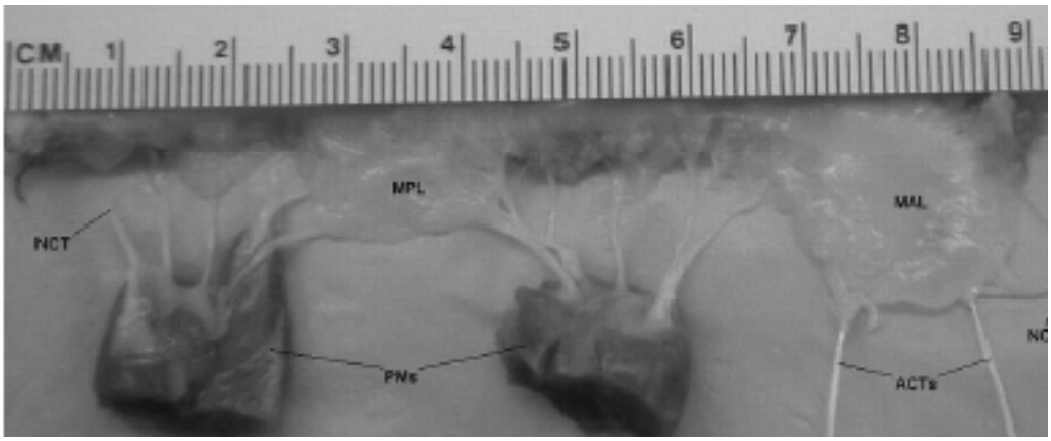

Figure 28: Distribution of chordae in the mitral valve, Source: (Bajona 2008)

The chordal distribution in our model was based on observations made during these dissections. The variability between person to person is such that an exact reproduction of chordal distribution of one individual is not representative of another. We therefore aim to model the mathematical equivalent to the chordal forces on the valve leaflets.

The anterior, posterior and commisure chordae were assumed to originate from three different points on the papillary muscle, as evident in Figure 28. The marginal chordae of each leaflet were however assumed to originate from a single point. (Figure 30). We chose not to model the branching of the marginal chordae, the exact pattern of which can get very intricate. Instead we modeled many marginal chordae originating at one point on the papillary muscle to represent the force exerted by the marginal chordae. This approximation should be fairly close to the branching network seen in reality. Also, this was a useful approximation in being able to

evaluate the tension in each set of marginal chordae (anterior, posterior and commisure) separately.

The chordae were modeled as tension only cables in LSDYNA. This ensures that the chordae only offer resistance to deformation when they are in tension. They also offer no resistance to rotation or bending. In the LSDYNA frame work, such cables are easily modeled using *MAT_CABLE card.

The thickness of the cross section of the chordae was accounted for in our model. Kunzelman reported cross section diameters of various chordae. (See table 2)

ANSYS was used as a pre-processor to LSDYNA. The geometric modeling was done completely in ANSYS while the material model was implemented in LSDYNA. LS-PREPOST was used for post processing.

Table 3: Diameter of various chordae, source: (K. Kunzelman 2007)

Chordae type	**Cross section (mm^2)**
Primary marginal	0.45
Primary basal	0.79
Strut chord	1.15

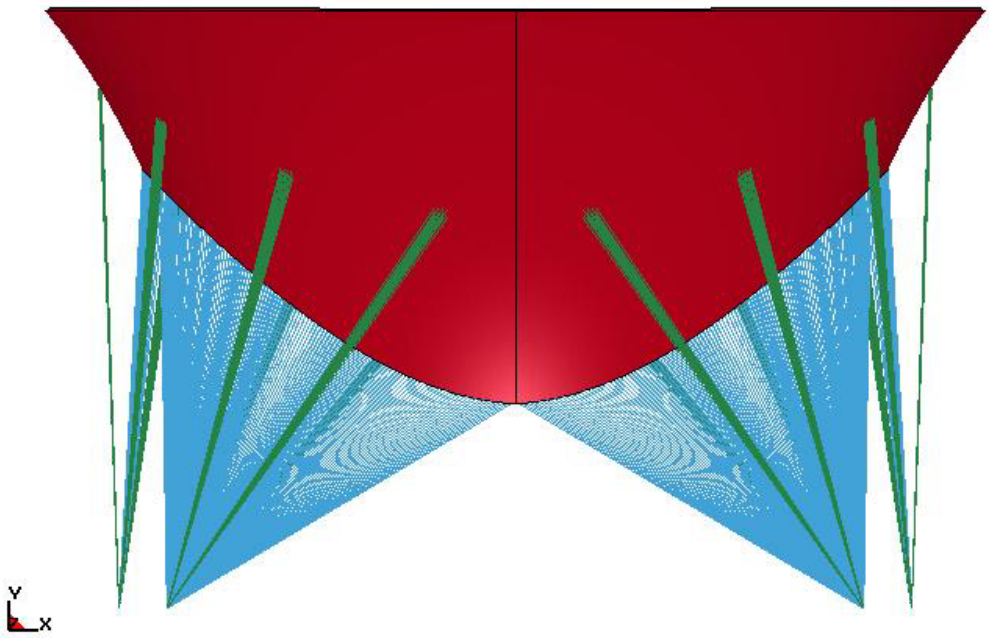

Figure 29: Mitral valve with chordae, front view

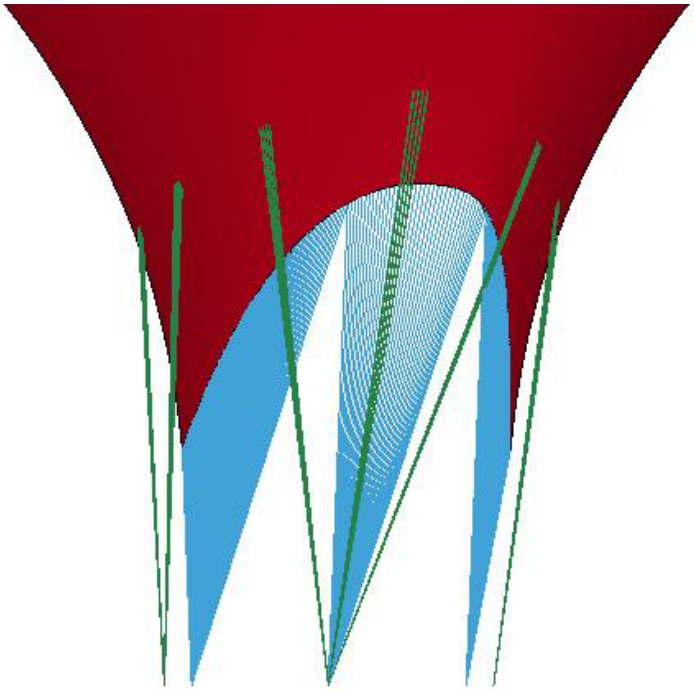

Figure 30: Mitral valve with chordae, side view

2.5 FINITE ELEMENT MODEL

After the material model was implemented in LSDYNA and material model parameters were fitted to experimental data, the geometric model was discretized to a finite element model.

The valve tissue material was meshed using linear 8 node brick elements. Since the elements are linear, i.e they can only represent the deformation field linearly and thus require a fine mesh for the analysis. The mitral valve tissue is meshed with 95,000 elements with two layers of elements through thickness.

The valve was meshed in mapped fashion such that the elements align in the circumferential direction. A local orthotropic coordinate system was used to identify the mean direction of the fiber in each element. A mean fiber direction in the circumferential direction was assigned.

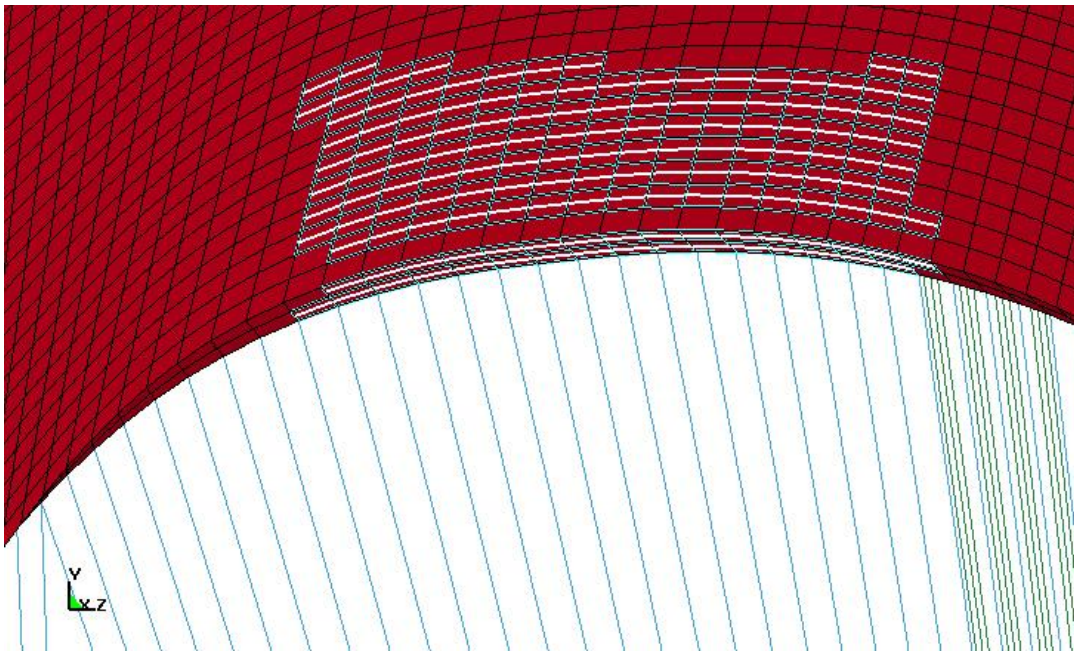

Figure 31: Mean fiber direction (white line) is in the circumferential direction

A fully integrated formulation rather than reduced integration is used for the solid element. This means that 8 integration points are placed in each corner of the brick element. Fully integrated elements are not prone to hourglassing. Typically fully integrated elements are too stiff because of volumetric locking and shear locking. However, since we have a multiplicative split in the strain energy volumetric locking in not an issue. Shear locking is possible but is not dominant in a bending dominant problem such as ours. The fully integrated formulation ensures three integration points through thickness so the transverse shears are modeled appropriately in a bending problem. (see Figure 32)

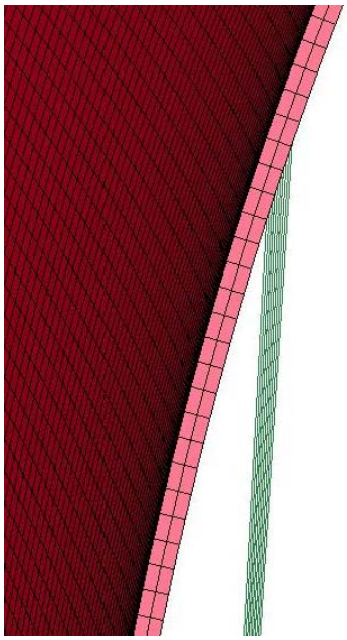

Figure 32: Three integration points through thickness of the valve

A pressure pulse of 140 mm-Hg (approx 18.5 kPa) is applied as surface pressure on the valve leaflets over a period of 0.125 s. (see Figure 46 for diagram of pressure pulse). We didn't model the unloading phase of the mitral valve. Nielsen et al. (NIELSEN 2004) measured tension values of various chordae at this loading. We will compare our computed tension values with their published measured data.

Constraints were applied to the annulus circumference and the papillary muscles to hold the mitral valve in place. Mitral annulus motion was neglected. The translation of papillary muscle as the left ventricle walls move was also neglected.

A transient explicit solution was obtained to the structural problem in the LSDYNA framework. The explicit algorithm doesn't check for convergence of solution, it uses a forward march algorithm that is stable as long as the time step of the calculation is sufficiently small. LSDYNA sets the time step at 90% of the speed of sound in the medium.

The solution is validated against a test problem to ensure that the solution obtained is reasonable. Since there is no convergence check on the model these validation tests are essential.

A half model was used to solve the actual finite element formulation because of the size of the model. Symmetric boundary condition was used at the interface where the model was split in two sections.

3.0 RESULTS

3.1 GROSS MOTION OF LEAFLETS

The overall motion of the leaflets is satisfactory. We observe that the anterior leaflet tucks under the posterior leaflet and pushes the posterior leaflet outward (see Figure 33). This happens because the annular attachment of the anterior leaflet is much straighter so this leaflet is almost freely hinged about the annulus. This has been observed previously by Kunzelman (K. Kunzelman 2007).

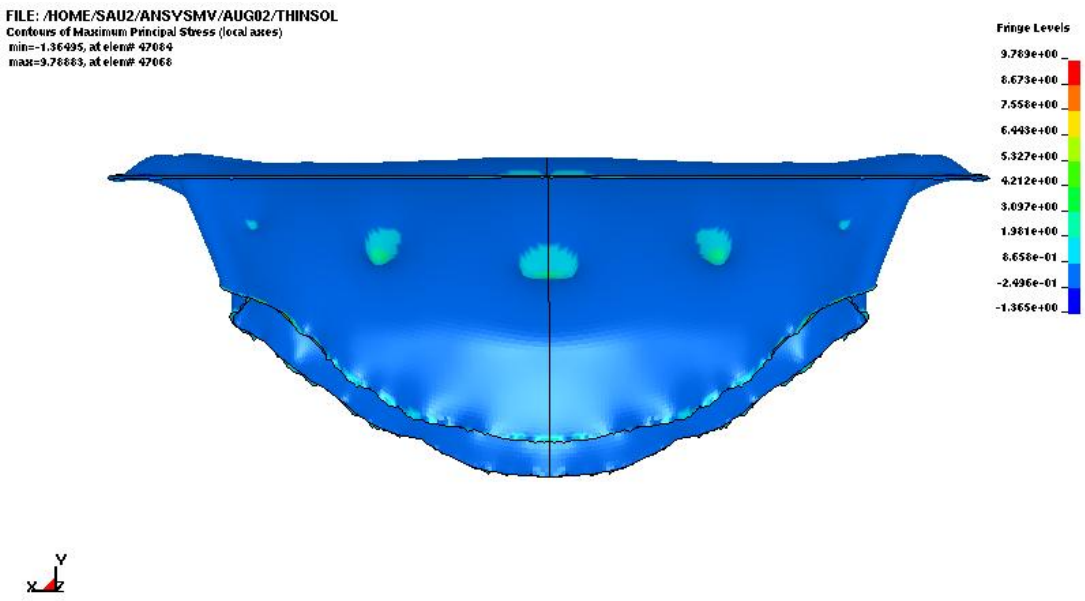

Figure 33: Anterior leaflet (forward) posterior leaflet (back)

Further, we plot the cross section of the leaflets over time. By plotting the cross section we can observe the leaflets as one would observe them in an echocardiograph. Note that, only a small portion of the leaflets actually come into contact with one another.

The manner in which the valve folds during coaption is also significant in being able to say whether the finite element model accurately captures the coaption process. Figure 40-Figure 45 show the top view of the valve which shows the scallops formed in the coaption process. The five scallops seen on the posterior leaflet also form in the finite element model, suggesting that the model is folding in a manner similar to that observed in nature.

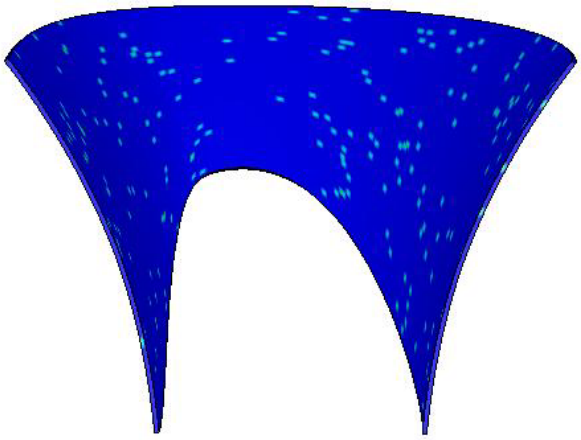

Figure 34: Cross section at t=0

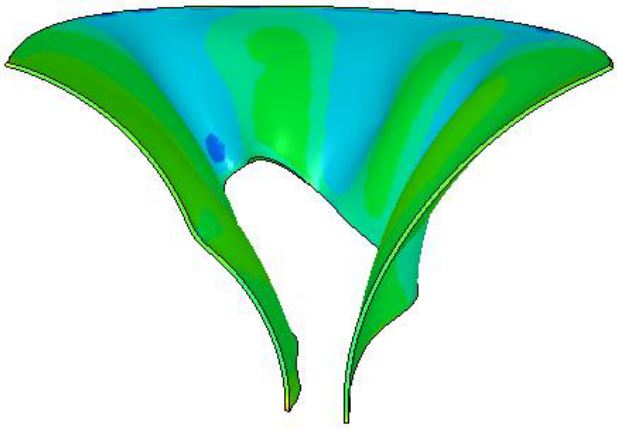

Figure 35: Cross section at t=0.02 s

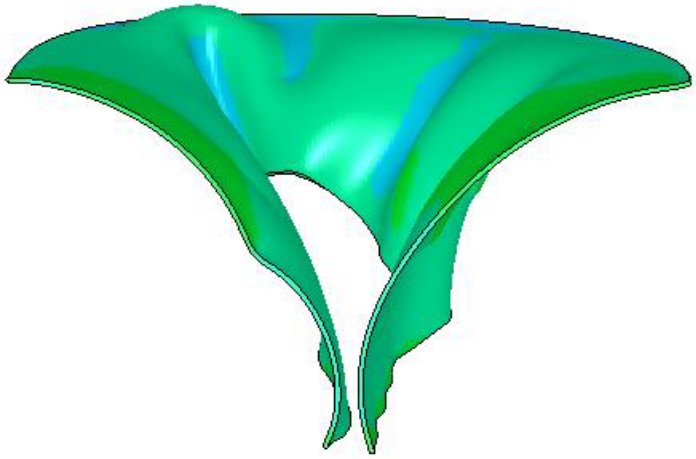

Figure 36: Cross section at t=0.04s

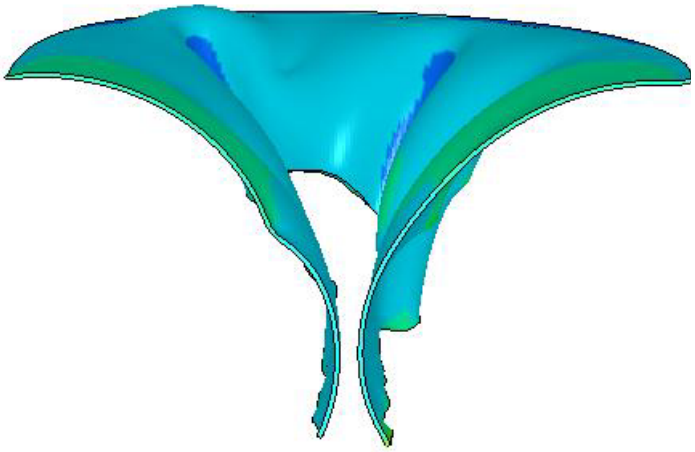

Figure 37: Cross section at t=0.06 s

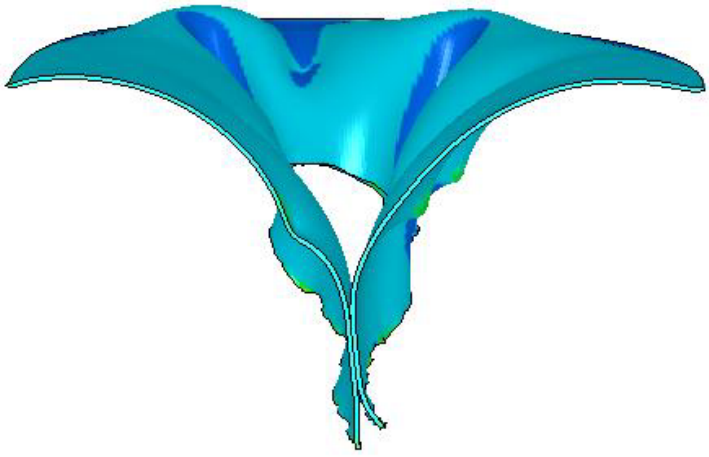

Figure 38: Cross section at t=0.08 s

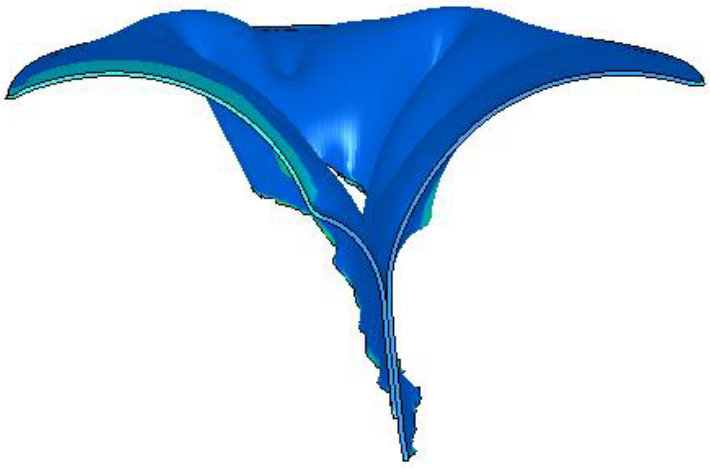

Figure 39: Cross section at t= 0.1s

A notable difference in the computed leaflet shape and actual shape lies in the curvature of the leaflet. Several factors contribute to a higher curvature in the computed leaflet shape. First, the fiber distribution and the annulus shape are approximate. It is likely if a more realistic fiber distribution was available, such as from SALS (Cochran 1991), the leaflet response could be stiffer.

A larger contributing factor to the computed shape of the leaflets is the fact that the annulus plane is assumed to be stationary. As a result, in the computational model, the work done in pushing the annulus plane has extra energy that goes into bending of the leaflets.

Another contributing factor is purely numerical. The bending stiffness of finite element models often depends on the finite element formulation. Mesh locking is often a problem with incompressible material formulations. To avoid that, the finite element solution ends up becoming "softer" than the real solution. Having stated the above limitations, the results are within acceptable engineering approximation because the leaflets bend in a manner that we observe in reality and the chordal forces are close to what would be expected in real chordae.

3.2 STRESS DISTRIBUTION

The stress history of the mitral valve leaflets was tracked from beginning of systole to mitral valve closure. As mentioned before, the relaxation phase of the mitral valve was not simulated, for the simple reason that peak stresses are not expected during this phase.

Peak stresses were observed at the points where the chordae attached to the leaflets. This was expected, as these are thin segments which transmit force to the leaflets and commisure; and stress tends to concentrate in the thin segments. The chordal attachment to the leaflet in reality can get very narrow and may require to be modeled as a point loads which results in very high stresses around the force application point. The chordal attachments to the leaflets were therefore distributed over multiple nodes instead of applying them at single points.

The peak stress noted by location are as follows:

Table 4: Peak stress at various locations

Basal attachment	2.6 Mpa
Marginal attachment	2.9 Mpa
Leaflet body	0.23-0.56 Mpa
Commisure	-0.3Mpa

The stress in the bulk of the leaflet was tensile from stretching of the leaflets. In the commisures the valve material folds, so most elements are under compression but some elements are in tension also. The basal and marginal attachments experience high tensile stress.

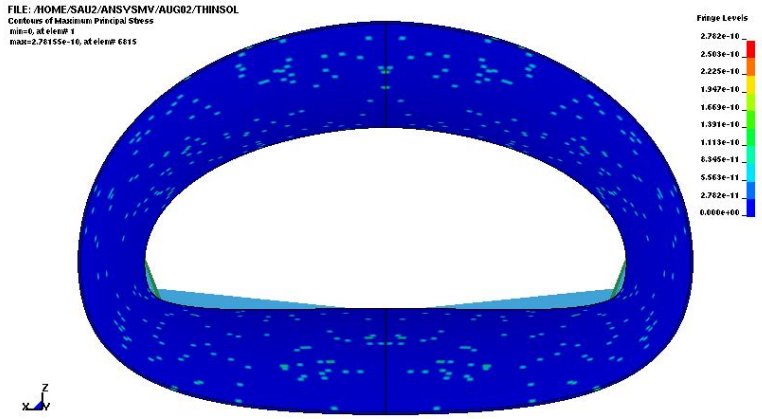

Figure 40: 1st principal Cauchy stress, t=0

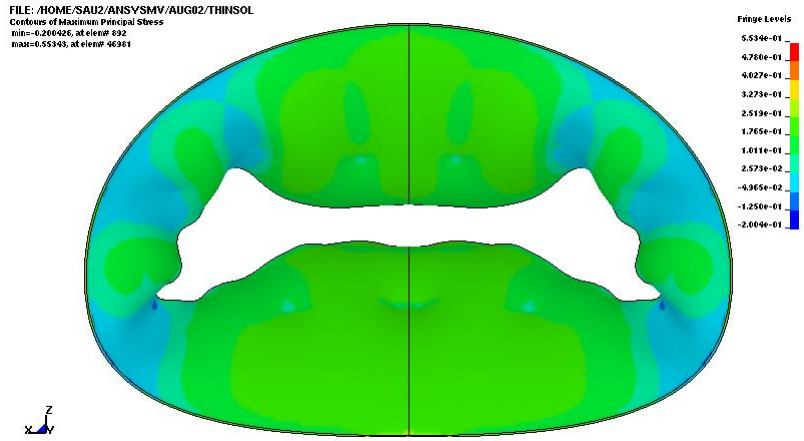

Figure 41: 1st principal Cauchy stress, t=0.02

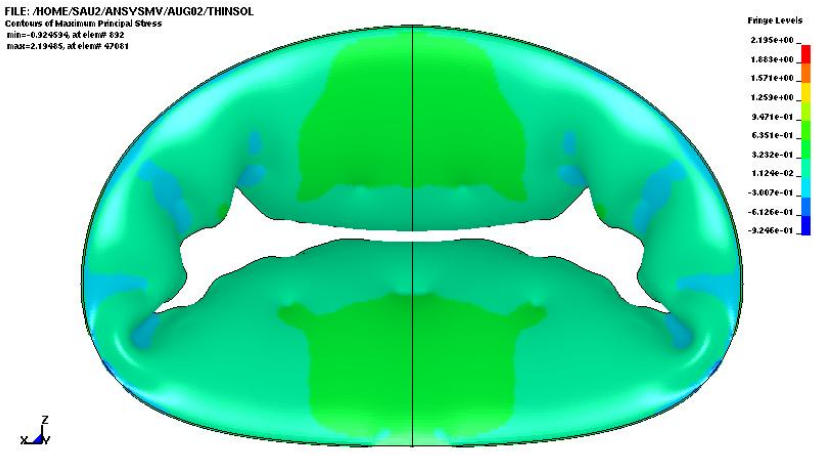

Figure 42: 1st principal Cauchy stress, t=0.04

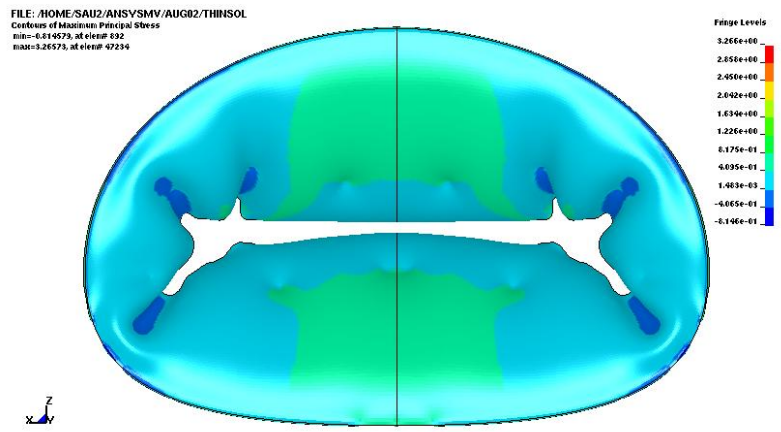

Figure 43: 1st principal Cauchy stress, t=0.06

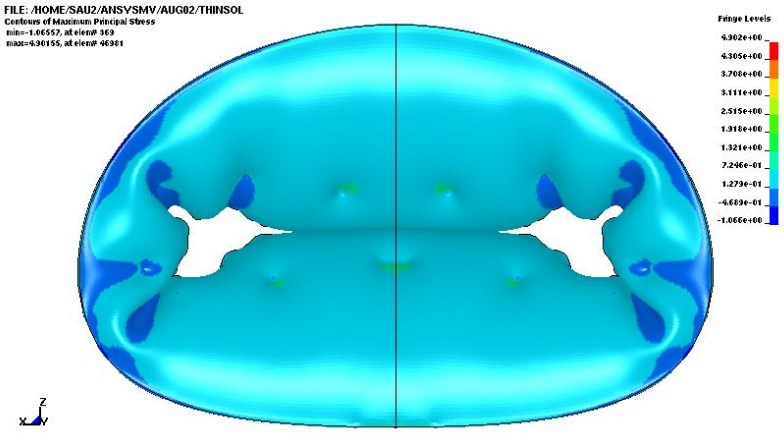

Figure 44: 1st principal Cauchy stress, t=0.08

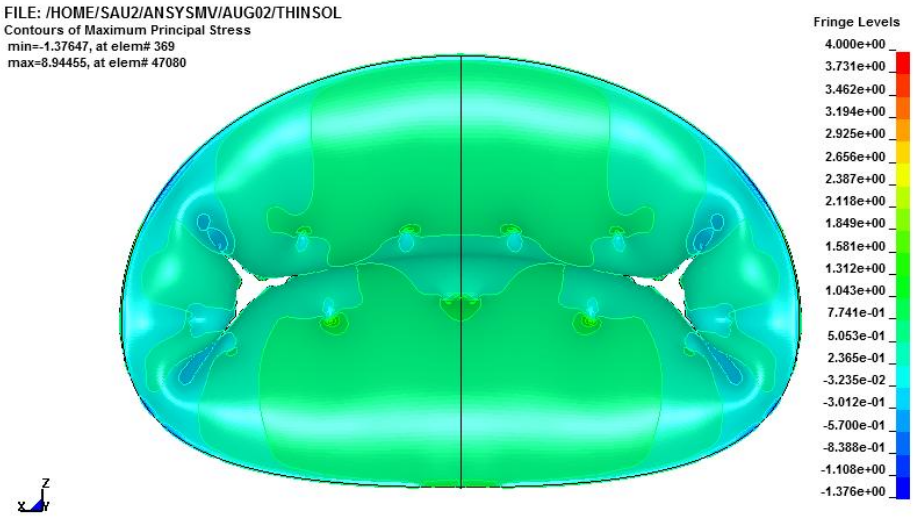

Figure 45: 1st principal Cauchy stress, t=0.1s

3.3 CHORDAL FORCES

The tension in various chordae and the net force exerted on the papillary muscle by the chordae during systole due to coaption is predicted by our model. The computed values were compared with the experiemental measurements by Nielson et al. (NIELSEN 2004) and are found to be in good agreement. Our computational model suffers from numerical oscillations, which were not damped out even though damping was introduced. The force data from the model therefore seems noisier than the experimentally measured. However, we were able to obtain reasonable agreement in the peak values of the tension.

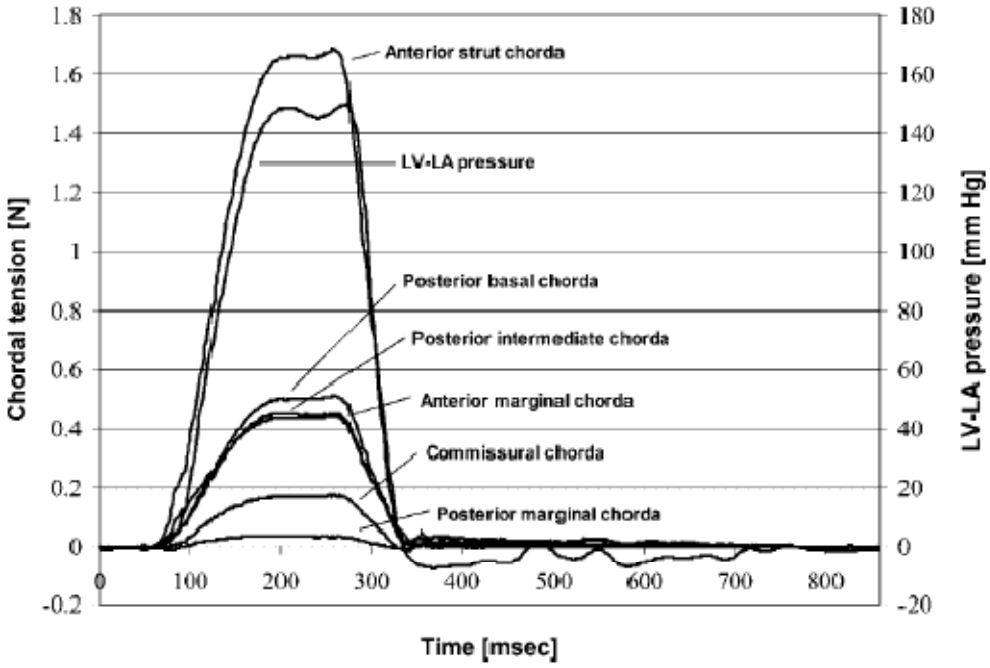

Figure 46: Measured tension in mitral valve chordae, source: (NIELSEN 2004)

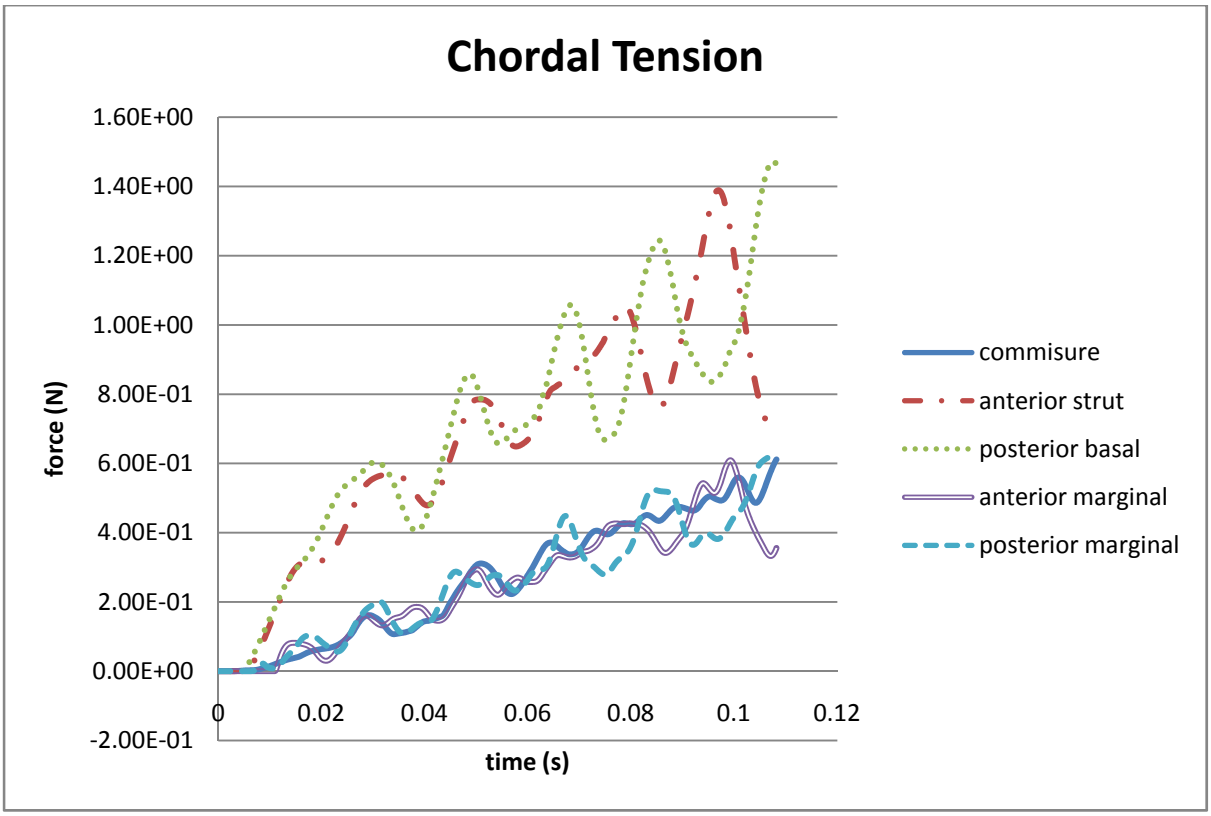

Figure 47: Computed chordae force

4.0 MODELING MITRAL VALVE PROLAPSE

To demonstrate the need for tension in mitral valve chordae for proper coaption, prolapse in both the leaflets was modeled by reducing the strength of all the chordae to insignificant values. It was observed that the leaflets collapsed under pressure but didn't hold their shape, and then prolapsed into the atrium. Figure 48, Figure 49 show the leaflets first collapsing under pressure and then falling into the atrium with no chordae to hold them in place.

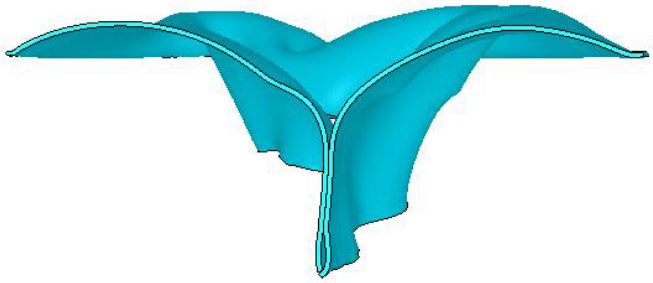

Figure 48: Cross section of leaflets, leaflets collapse under pressure at t=0.06 s

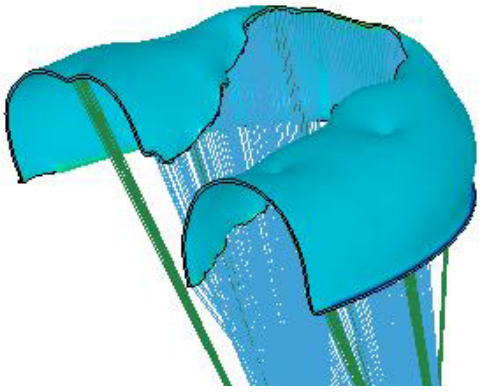

Figure 49: Cross section of leaflets, leaflets prolapsed into atrium at t=0.1 s

In an experiment performed by Bajona et al. (Bajona 2008) mitral valve prolapse was induced by cutting chordae supporting the aortic leaflet. Artificial chordae were then surgically implanted and the prolapse was fixed. In order to achieve the same prolapsing leaflet in their experiment, we removed all constraints on the aortic leaflet and allowed the finite element model to solve for physiologic loading conditions. We observed that the aortic leaflet in the computational model also prolapsed into the atrium without support of the chordae. Figure 50 shows the leaflet shape of a prolapsing leaflet.

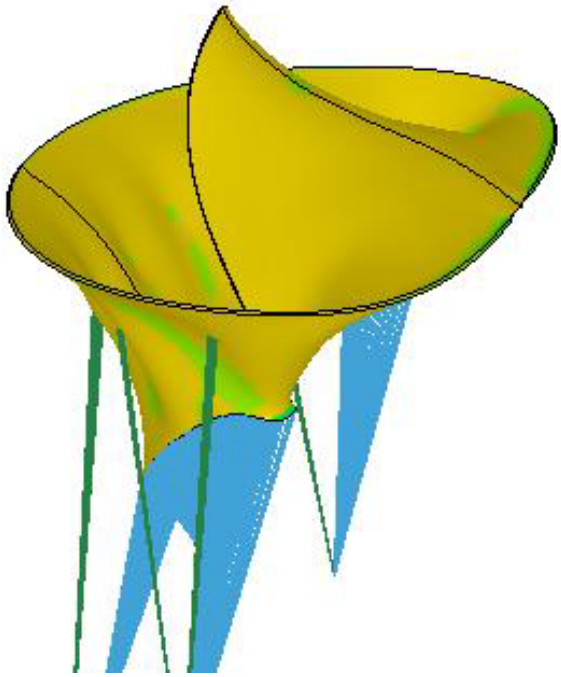

Figure 50: Prolapsing aortic leaflet

5.0 MODELING SURGICAL REPAIRS

The innovative surgical procedure described in (Bajona 2008) was modeled. In this procedure a Gorotex suture is tied to the free edge of the prolapsing anterior leaflet and tension adjusted such that the valve doesn't regurgitate.

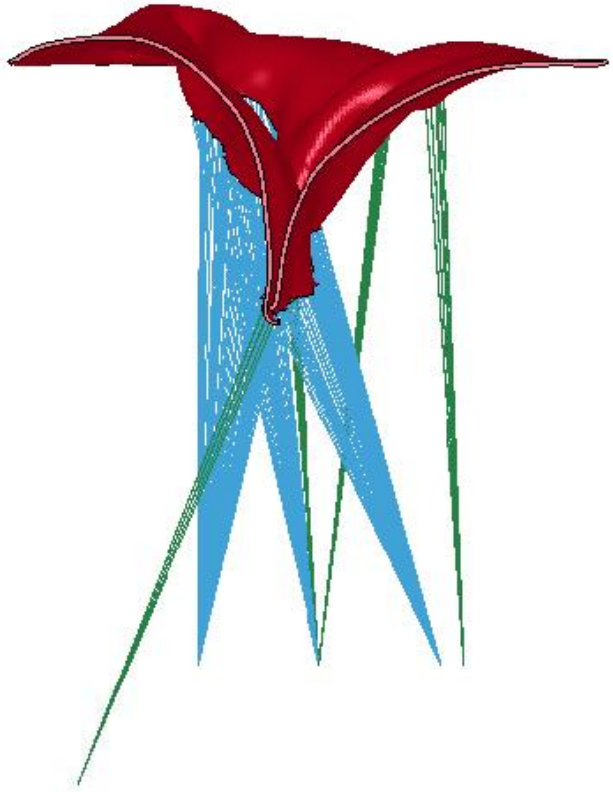

Figure 51: Cross section of mitral valve with surgical repair

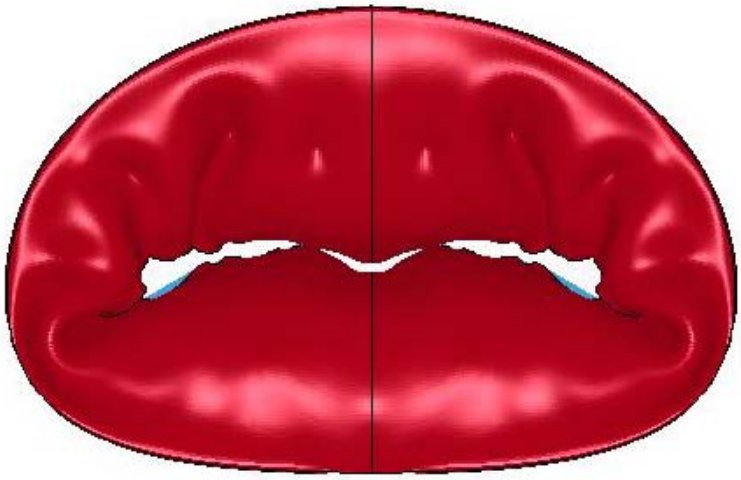

Figure 52: MV after surgical repair top view

As seen from Figure 51, Figure 52 it is possible to tie a suture to the valve leaflets so that the prolapsing leaflet is held in place and there is no regurgitation. However, since the location of attachment is different from natural, it is going to cause an altered state of stress in the leaflets.

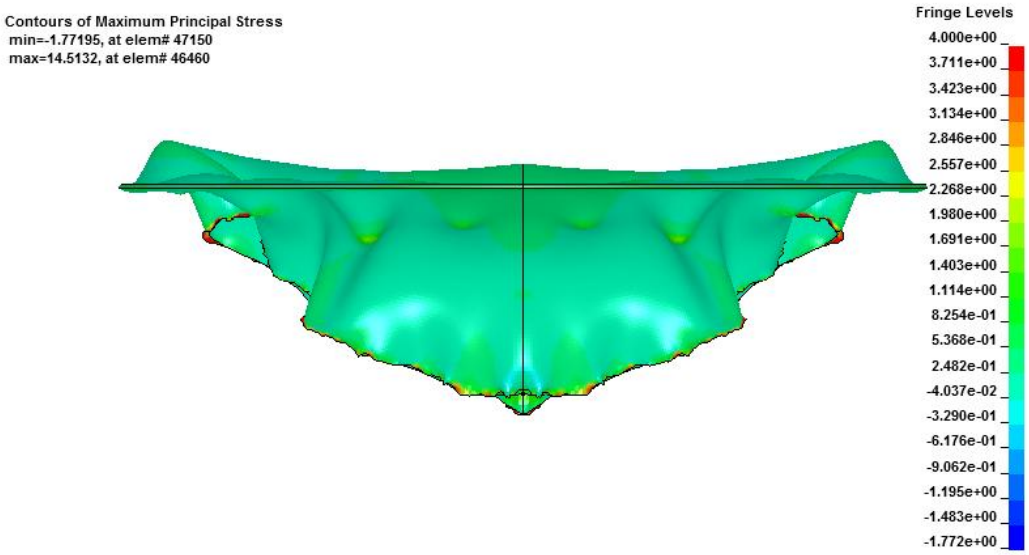

Figure 53: State of stress after surgical alteration (front view)

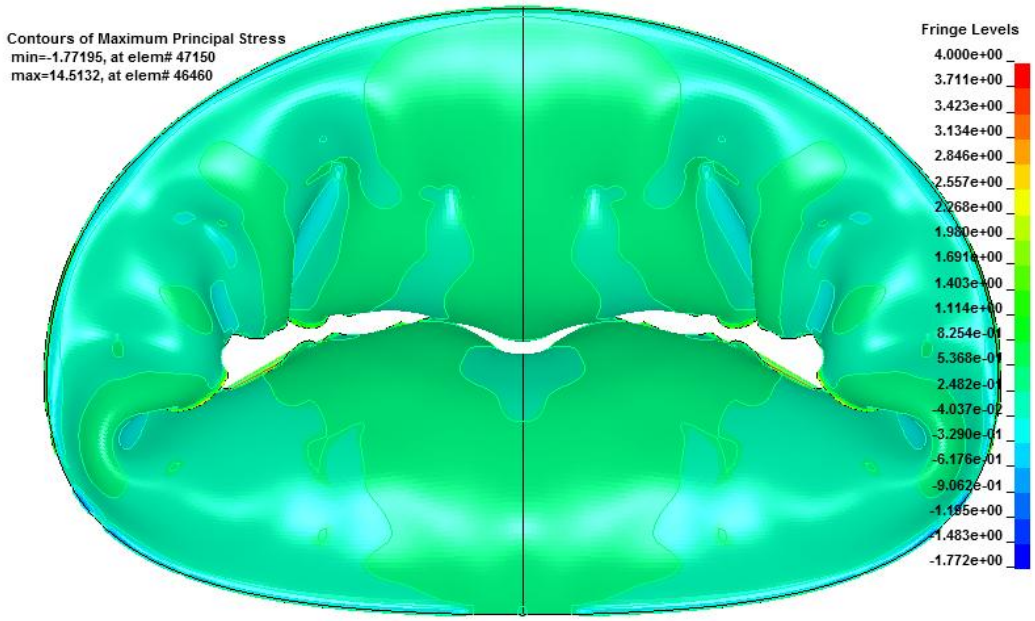

Figure 54: State of stress after surgical alteration (top view)

Highest first principle stress was observed at the point where the suture was tied to the valve. (~6Mpa) and the sites where marginal chordae attach to the free edge were also locations of high stress. Surprisingly, the elements in the belly of the mitral valve experienced a reduced state of tensile stress. This is possibly because of lack of constraints the material didn't stretch as much at the belly of the valve.

Table 5: Stress at various locations before and after surgery

Location	Pre-surgery	Post-surgery
Basal attachment	2.6 Mpa	1.5 Mpa
Marginal attachment	2.9 Mpa	6.0 Mpa
Leaflet body	0.23-0.56 Mpa	0.18-0.3 Mpa
Commisure	-0.3 Mpa	-0.17 Mpa

6.0 REMODELING – CHANGE IN FIBER DIRECTION

Comparing the principal directions of stress and strain at all locations of the valve is going to be impractical. However, we can monitor a certain location of the valve that we are interested in to see if the principal directions of strain and stress have changed post surgery. Pre-surgery valve principal stress directions are given in Figure 55. The post surgery valve principal stress directions are given in Figure 56.

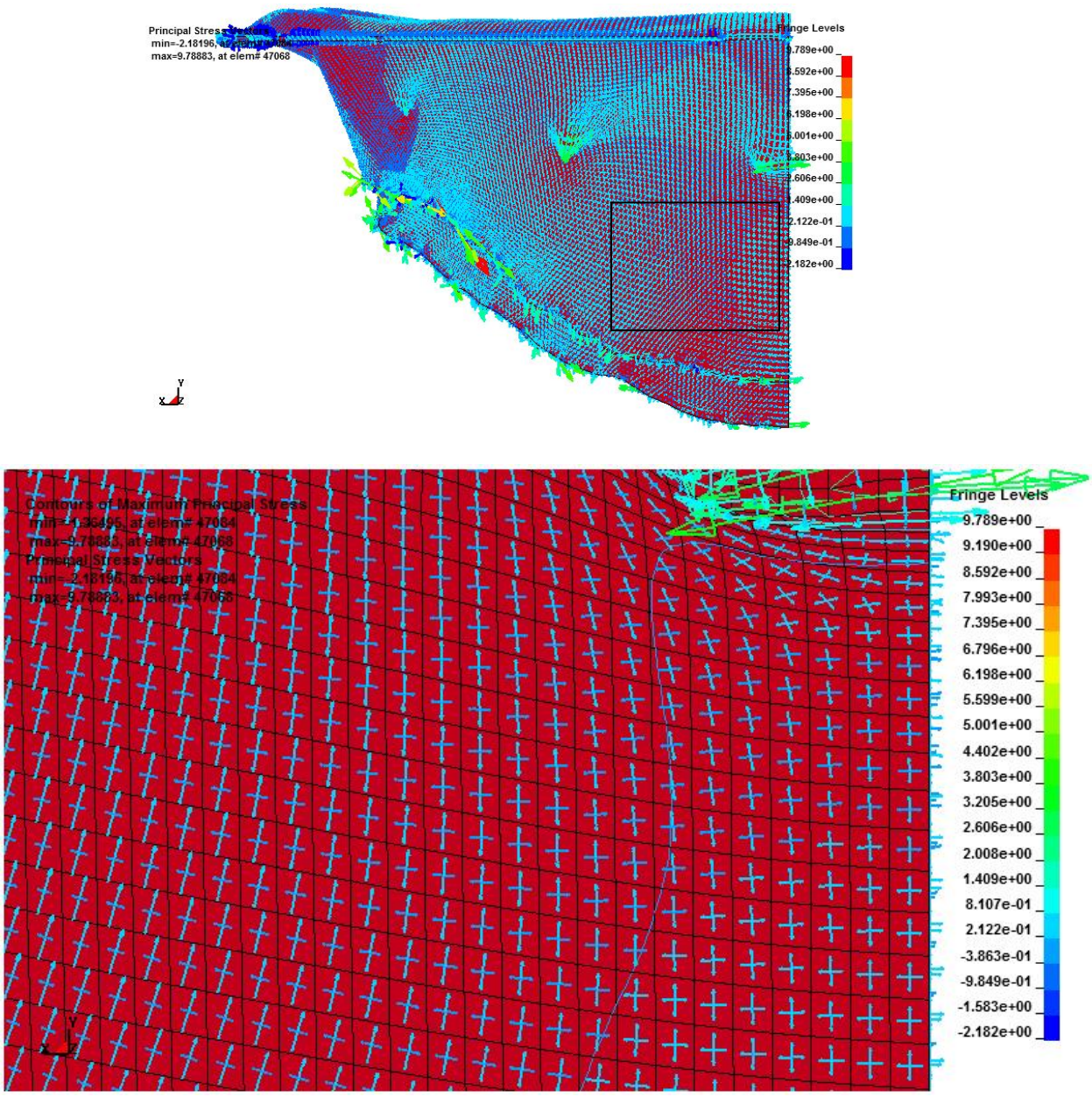

Figure 55: Principal stress directions in AV leaflet section

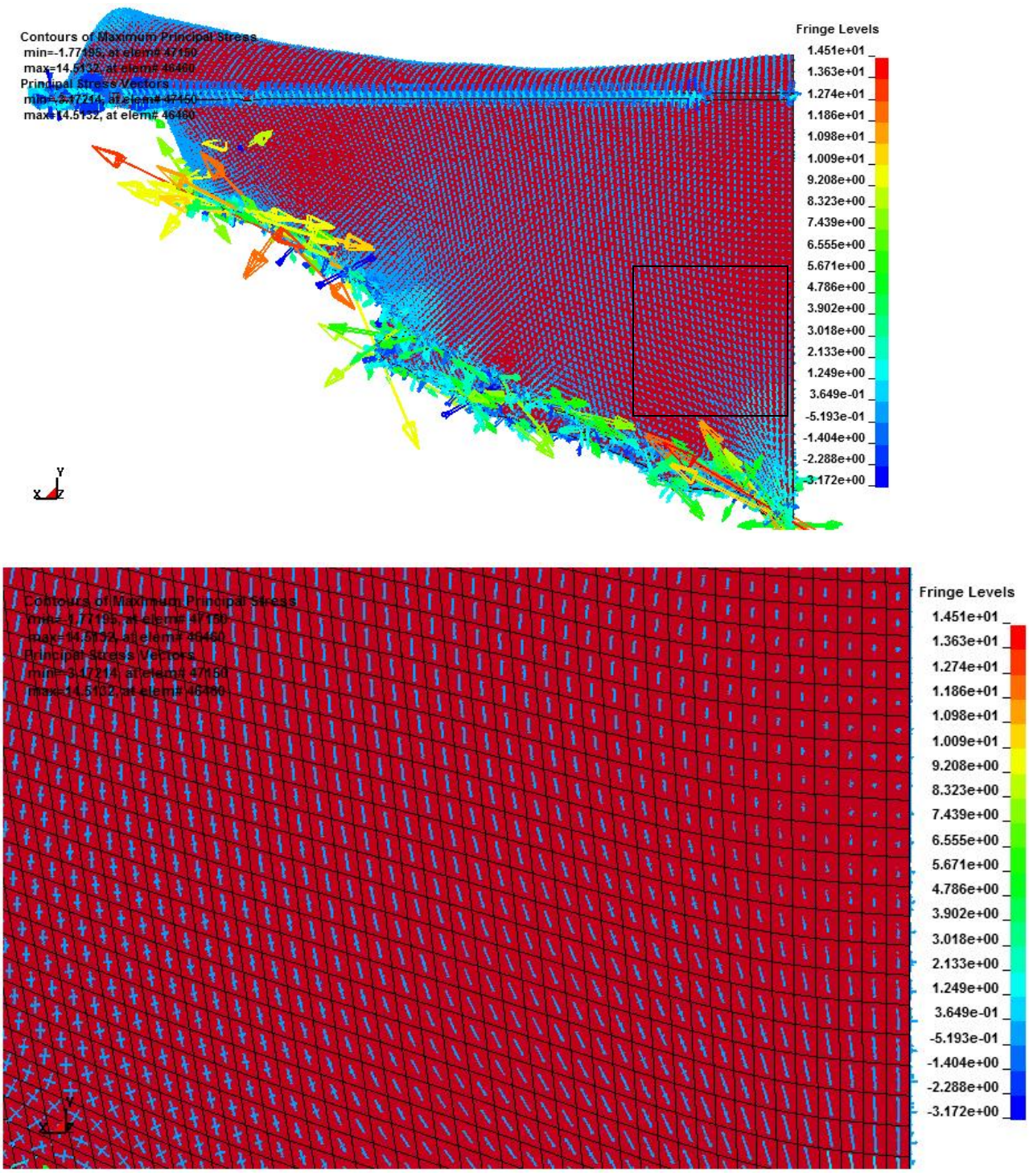

Figure 56: Post surgery principal stress directions in AV leaflet section

Evident from Figure 55 and Figure 56 is the difference in the principal stress directions. Most notable is the difference in the development of the second principal direction of stress,

whereas pre-surgery, in the natural configuration where there were more than one basal attachments the material stretched such that both the first and second principal directions of stress developed, almost as though the material was experiencing a biaxial state of stress (as seen in a biaxial testing setup for instance).

In the post surgery valve, only the first principle stress develops the second principal stress is negligibly small. As the material is held at only one location, the material is stretched from one point and the first principle direction of stress points to the attachment point of the chordae to the valve.

Taber and Humphrey (Taber and Humphrey, Stress modulated growth, residual stress and vascular heterogeneity 2001) discuss a connection between the stress in tissue, it's anisotropy and remodeling. Although their models primarily address tissue in arteries, it is our assumption that the remodeling in valve tissue is similar to these theories. That is to say, remodeling in mitral valve tissue is assumed to be stress modulated. We further assume that the fiber direction will change so as to minimize the stress in the tissue. This can be best achieved if the fiber direction aligned to match the maximum principal direction.

The change in principle direction thus reflects a change in fiber direction. To compute the exact change in fiber angle is a challenging task. In the case of arteries it has been shown that the most optimum fiber configuration is a double helix through the artery (Hariton, et al. 2007). In the case of mitral valve no shown special configuration is known to exist. The valve in its healthy state has fibers more or less oriented in the circumferential direction. In the case of the mitral valve any surgical alteration that changes the principal stress direction is likely to alter the fiber orientation.

7.0 WHAT-IF STUDY

The surgical intervention described by Bajona et al. (Bajona 2008) was modeled and its effects predicted in terms of altered stress state and changed principal stress directions. Our finite element study shows greater stress at the marginal chordae but reduced stress in the leaflet body. Also, the second principle direction is much lesser after surgery, indicating that the mitral valve tissue doesn't undergo the same biaxial nature of stress as it would have without intervention.

Clearly, one option available to the surgeon is to place the attachment point of the artificial chordae (suture) as close to the attachment point of the damaged native chordae as possible. If tension in the chordae is similar to the native chordae then the chance of remodeling is minimized.

However, during a minimally invasive surgery it is rarely possible to accurately place the suture at a given attachment point. In order to implant the artificial suture in a minimally invasive surgery, we worked on designing specialized instruments that would stitch the suture to the valve. At present we are able to successfully tie the suture to free end of the mitral valve only. Significant amount of time and energy is being spent in the development of another surgical tool so we could implant the suture in the belly of the mitral valve. However, as of now, there is no clear evidence that a artificial suture implanted in the belly of the mitral valve is better than placing the attachment at the free edge.

In order to compare the merits of placement at these two locations, a what-if study was considered. The basal attachments to the anterior leaflet were removed in the finite element model while keeping the marginal attachments. The suture was then tied between the free edge of the anterior leaflet and a point on the left ventricle. The focus is on how well the leaflets coapt. The same procedure was tried again with the artificial chordae tied to the belly of the anterior leaflet.

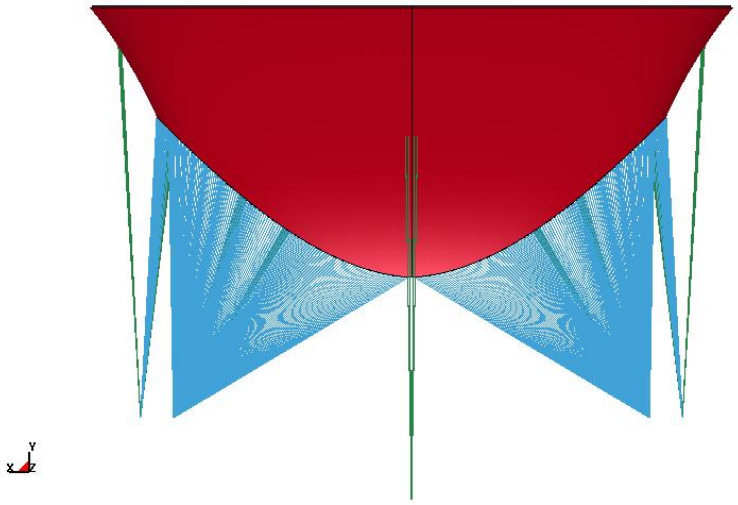

Figure 57: Artificial chordae attached to belly section

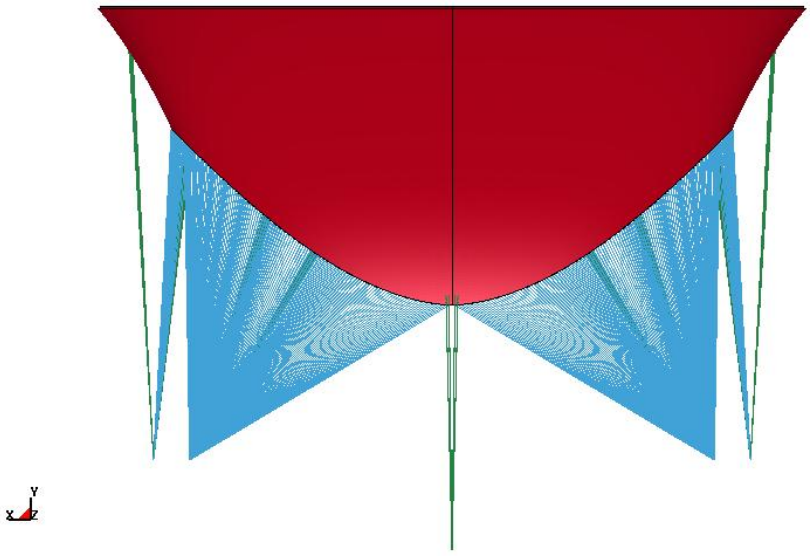

Figure 58: Artificial chordae attached to free edge

Figure 57and Figure 58 show the artificial chordae attached to the belly and free edge respectively. The results from suture attachment at the free end have been presented in Table 5. The results from the artificial chordae attached at the belly are presented below.

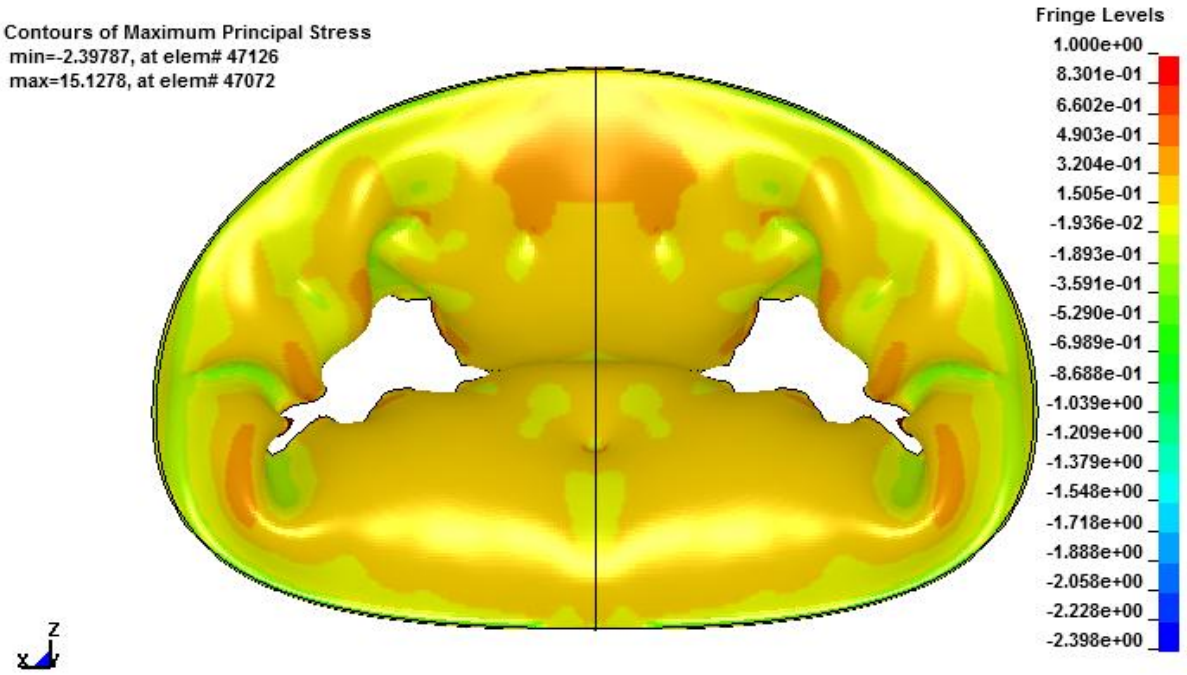

Figure 59: Improper coaption of MV leaflets

Table 6: Stress distribution in leaflets after suture is attached at belly of anterior leaflet

Basal attachment	0.5 MPa
Marginal attachment	3 Mpa (some locations 7MpA)
Leaflet body	0.15 Mpa ~0.3 Mpa
Commisure	-0.8 Mpa ~-1 MPa

As can be seen from Figure 59, the leaflets didn't coapt properly when the suture was attached to the belly of the anterior leaflet. Proper coaption is the first order of business for the surgical team as they are looking to primarily restore the cardiac sufficiency of the patient with a regurgitating valve.

The direction of the principal stresses is given below:

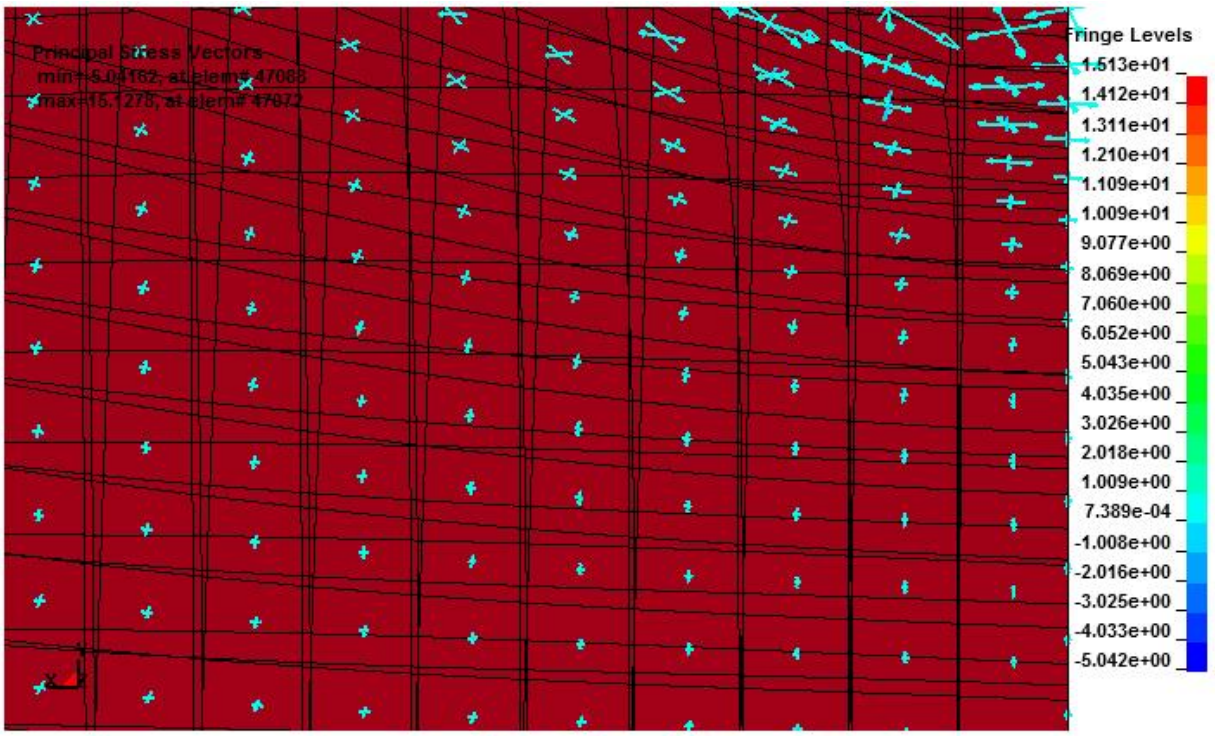

Figure 60: Principal direction of stress for leaflet with suture attached at belly

Figure 60 suggests that the principal directions of stress in this case as slightly closer to that would be in the natural state. First and second principal stresses at comparable magnitudes. However, since the coaption of the valve after this surgery is poor, further considerations for this surgery are not required.

8.0 LIMITATIONS

The splay was assumed to be a constant in our study, but it has been shown that the fibers tend to be more tightly distributed about the mean at higher strains. It is virtually impossible to map the fiber splay at each material point at every instant, and even if we do this for a single mitral valve the results may not apply in general to all valves. More detailed structural theories are required to explain the behavior of the collagen fibril.

Without the access to the SALS data of entire valves, we used only an approximate fiber distribution based on a representation by Cochran et al. (Cochran 1991).

Shear coupling terms in the constitutive model remain to be accounted for. The shear stresses generated in our model come from the isotropic portion of the material model, no coupling terms are defined to capture the interaction between the fiber and matrix. In effect we are making the approximation that the presence of the collagen fibers affects only stiffness in the fiber direction in tension.

Thickness of the valve material is not uniform throughout the valve as we have assumed. Sometimes the valve tissue can by lumpy at locations. This change in thickness need to be accounted for in the next generation of models.

9.0 SUMMARY AND FUTURE RESEARCH

We have developed constitutive equations that included the effects of collagen fibers in representing (within reasonable approximations) the behavior of mitral valve tissue. Having developed these constitutive equations we further implemented them in a commercial finite element code, LS-DYNA. The complex geometry of the mitral valve was modeled using prior published data as well as the complex chordal distribution that we observed in the laboratory. We were able to visualize the folding of the mitral valve leaflets under different loading conditions in our finite element solution. If the structural supports of the chordae were removed from the anterior leaflet a prolapsed leaflet was observed. Further, a weakening of all the chordae showed that both the leaflets prolapsed into the atrial side.

Replacing the removed natural chordae with artificial sutures at the free edge of the anterior leaflet, we modeled a novel surgical procedure and observed that if the surgical correction produced an appropriate folding of the mitral valve. We also observed changes in the principal directions of stress post surgery, which according to stress modulated theory is a major indicator of future collagen remodeling.

An alternative location for placement of the artificial chordae was tried for the surgical correction (in the belly of the anterior leaflet) as a means to reduce collagen remodeling, however, the alteration did not yield a proper coaption. Hence, via our computational model we showed that the belly attachment of the suture will not produce a coaption as efficient as that by

attaching the chordae to the free edge. However, the principal directions of stress is less altered from natural state in this latter option. Therefore, placing the suture at the belly may have its advantage but unless we ensure correct coaption the surgery will not solve the problem of regurgitation which is the main goal of such surgery.

For future research, in order to calculate the actual remodeling of the collagen fibers in the mitral valve leaflets an optimization study would be very informative. In arteries, the collagen fibers are known to realign in order to minimize the circumferential stress in the artery. (Taber and Humphrey 2001) In the same respect an objective function from stress consideration can be identified for the valve leaflets and optimum fiber locations computed.

Another useful future research would be to introduce fluid structure interaction if one is interested in the dynamic effects of fluid flow within the ventricle and it's interaction with the valves and the chordae.

BIBLIOGRAPHY

Ansys Inc. http://www.ansys.com.

Bajona, Pietro. "Tension Measurement of Artificial Chordae Tendinae Implanted Between the Anterior Mitral Valve Leaflet and the Left Ventricular Apex An In Vitro Study." *Innovations*, 2008.

Billiar, KL, and MS Sacks. "A method to quantify the fiber kinematics of planar tissues under biaxial stretch." *Journal of Biomechanics*, 1997: 753-756.

Cochran, RP. et al. "Nondestructive analysis of mitral valve collagen fiber orientation." *ASAIO Trans. 37*, 1991.

Dagum, P. et al. "Coordinate free analysis of mitral valve dynamics in normal and iscemic hearts." *Circulation*, 2000.

Dal, Pan et al. "Structural effects of an innovative surgical technique to repair heart valve defects." *J. Biomech*, 2005.

Einstein, DR. "Nonlinear accoustic analysis of the mitral valve." 2002.

Fung, Y.C. *Mechanical properties of living tissuees.* New york: Springer-verlag, 1993.

Grashow, JS. "Evaluation of Biaxial properties of the mitral valve anterior leaflet under physiologic loading conditions." *MS thesis.* 2002.

Green, AE. *large elastic deformations.* Oxford: Calendron, 1970.

Hariton, I, G deBottom, TC Gasser, and GA Halzapfel. "Stress driven collagen fiber remodeling in arterial walls ." *Biomechan Model Mechanobiol*, 2007.

Hayek E., Gring C.N.,Griffin B.P,. "Mitral Valve prolapse [review]." *Lancet*, 2005.

Holzapfel, GA Gasser TC. "A new constitutive framework for arterial wall mechanics and comparative study of material models." *Journal of elasticity*, 2000: 1-48.

Humphrey, J.D. *Cardiovascular solid mechanics.* New york: Springer-verlag, 2001.

HYUNGGUN, KIM, B KRISHNAN, MS SACKS, and LU JIA. "An Experimentally Derived Stress Resultant Shell Model for Heart Valve dynamic simulation." *annals of biomedical engineering* , 2007.

Kunzelman, KS. "Fluid structure interaction models of the mitral valve." *Phil. Trans. R. Soc. B*, 2007.

Kunzelman, KS. "Anatomic basis for mitral valve modeling." *Journal of Heart Valve Disease* 3 (1994): 491-496.

Liao. "The relation between collagen fibril kinematics and mechanical properties in the mitral valve anterioir leaflet." *Journal of Biomechanical engineering*, 2007.

lsopt. 2008. http://www.lsoptsupport.com/examples/parameter-identification.

May-Newman, K , Yin FCP. "A constitutive law for mitral valve tissue." *Journal of Biomechanical engineering*, 1998.

Prot, V. et al. "Finite element analysis of the mitral apparatus: annulus shape effects and chordal force distribution." *Biomechan Model Mechanobiol*, 2007.

Sacks, M.S. "Biaxial Mechanical Evaluation of Planar Biological Materials." *Journal of Elasticity*, 2000: 199-246.

Simo, J.C. "Variational and Projection methods for the volume constraint in finite deformation elastoplasticity." *Computer methods Applied Mechanical engineering*, 1985.

Spencer. *Continuum theory of mechanics for fiber reinforced composites.* New York: Springer-verlag, 1984.

Sussman, T. , Bathe K.J. "A finite element formulation for nonlinear incompressible elastic and inelastic analysis." *comput. struct.*, 1987.

Taber, LA. *The Nonlinear Theory of elasticity Applications in Biomechanics.* singapore: world scientific publishing, 2004.

Taber, LA, and JD Humphrey. "Stress modulated growth, residual stress and vascular heterogeneity." *Journal of Biomech engr.*, 2001.

Truesdell, C. "The mechanical foundations of elasticity and fluid dynamics." *Continuum Mechanics I* (Springer), 1966.

weiss, J. et al. "Finite element implementaion of incompressible, tranversely isotropic hyperelasticity ." *computer methods in applied mechanics and engineering*, 1996.

Wilcox, Cook , Anderson. *Surgical anatomy of the heart.* Cambridge University Press, 2005.